Acta Geotechnica
https://doi.org/10.1007/s11440-021-01389-1

RESEARCH PAPER

Energy equation and stress–dilatancy relationship for sand

Ching S. Chang[1] · Yibing Deng[1]

Received: 10 June 2021 / Accepted: 10 October 2021

Abstract
The energy equation is an expression of the first law of thermodynamics or the law of conservation of energy. According to the first law of thermodynamics, the externally applied work to a system is equal to the sum of dissipation energy and Helmholtz free energy of the system. However, most of the currently available stress–dilatancy relationships are based on the energy equation of Taylor-Cam Clay type, which hypothesizes that the applied plastic work is equal solely to the frictional dissipation energy. The Helmholtz free energy has been completely neglected. Recently, observed from acoustic experiments, it has been recognized that Helmholtz free energy can be caused by deformation mechanisms other than friction between particles. Thus, it is necessary to include additional terms in the energy equation in order to correctly model the stress-dilatancy behavior. This paper addresses the issue regarding the balance of this energy equation. Analyses of experimental results are presented. Specific forms of the frictional energy and Helmholtz free energy are proposed. The proposed energy equation is verified with the experimental data obtained from Silica sand, Ottawa sand, and Nevada sand.

Keywords Dissipation energy · Helmholtz free energy · Sand · stress–dilatancy relationship · Thermodynamics

1 Introduction

The stress–dilatancy relationship plays an important role in modeling the stress–strain behaviors of granular materials [24, 30, 56]. It is fundamentally connected to the laws of thermodynamics. Using both the First and Second Laws of Thermodynamics, the Clausius–Duhem inequality is given by Lemaitre and Chaboche [29]:

$$\Phi = \sigma_{ij}\dot{\varepsilon}_{ij} - \dot{\Psi} - s\dot{T} - \frac{Q_k T_{,k}}{T} \geq 0 \tag{1}$$

The dissipation energy Φ is the mechanical work input $\dot{W} = \sigma_{ij}\dot{\varepsilon}_{ij}$, subtracting the Helmholtz free energy $\dot{\Psi}$, the thermal energy $s\dot{T}$, and the thermal dissipation $\frac{Q_k T_{,k}}{T}$, where σ_{ij} is stress, ε_{ij} is strain, T is temperature, s is entropy, and Q is heat. The Clausius–Duhem inequality implies the thermodynamic admissibility of any non-dissipative processes. The thermal dissipation $-\frac{Q_k T_{,k}}{T}$ is small compared to the mechanical dissipation for slow processes, and hence it can be neglected [22]. The Clausius–Duhem inequality now reduces to a more stringent form.

$$\Phi = \sigma_{ij}\dot{\varepsilon}_{ij} - \dot{\Psi} - s\dot{T} \geq 0 \tag{2}$$

For isothermal condition $\Phi = \sigma_{ij}\dot{\varepsilon}_{ij} - \dot{\Psi} \geq 0$. Thus, the externally applied work $\dot{W} = \sigma_{ij}\dot{\varepsilon}_{ij}$ is equal to the summation of Helmholtz free energy $\dot{\Psi}$ and the dissipation energy Φ.

$$\dot{W} = \dot{\Psi} + \Phi \tag{3}$$

According to the second law of thermodynamics, the dissipation energy Φ is non-negative, which is vanished from the system via mechanisms such as frictional dissipation and particle breakage dissipation. In this manuscript, we study the dilatancy of sand under low confining stress, in which, the dissipation energy is primarily due to friction. The dissipation energy due to particle breakage is not considered.

In Eq. (3), the Helmholtz free energy $\dot{\Psi}$ can be either positive or negative (stored into or released from the system, respectively). In the conventional elastoplastic theory, the Helmholtz free energy consists of only elastic energy.

✉ Ching S. Chang
cchang@engin.umass.edu

✉ Yibing Deng
yibingdeng@engin.umass.edu; yibingdeng@outlook.com

[1] Department of Civil and Environmental Engineering, University of Massachusetts, Amherst, MA 01003, USA

Published online: 17 November 2021

However, the Helmholtz free energy stored in the system generally consists of both elastic energy and plastic energy.

For example, during volume contraction of soil under applied load, the elastic part of the applied work is stored in the system (i.e., elastic Helmholtz free energy). The plastic part of the applied work has two portions: A large portion is dissipated through friction, and the remaining portion is stored in the system through non-dissipative rearrangement of particles (causing an increase in potential energy). The stored plastic work would increase the plastic Helmholtz free energy in the system, which can be released during soil dilation at later stage.

Separating the total work into elastic and plastic components [52], the rate of elastic and plastic work can be written as

$$\dot{W}^e = \dot{\Psi}^e \tag{4}$$

$$\dot{W}^p = \dot{\Psi}^p + \Phi \tag{5}$$

Thus, part of the applied plastic work is dissipated and the other part is Helmholtz free energy which can either be stored in or extracted from the system.

Dissipation energy includes friction and breakage. In this paper the breakage is not considered. The experimental triaxial test data selected for this study were under small confining stresses.

Taylor [49] first discussed the basic idea of his famous "stress-dilatancy" theory from the energy perspective, by using a few data from direct shear tests on Ottawa standard sand. Taylor's intuitive assumption is based on the interpretation of incremental work done in a direct shear test,

$$\dot{W} = \tau \mathrm{d}u_h + \sigma' \mathrm{d}u_v \tag{6}$$

In this expression, σ' and τ are, respectively, the normal (effective compressive) and shear stresses, acting on planes parallel to the shear-plane, and u_h and u_v are, respectively, the relative horizontal and vertical displacements. The increment work is the amount of energy per unit area for the depth of shear zone (Fig. 1).

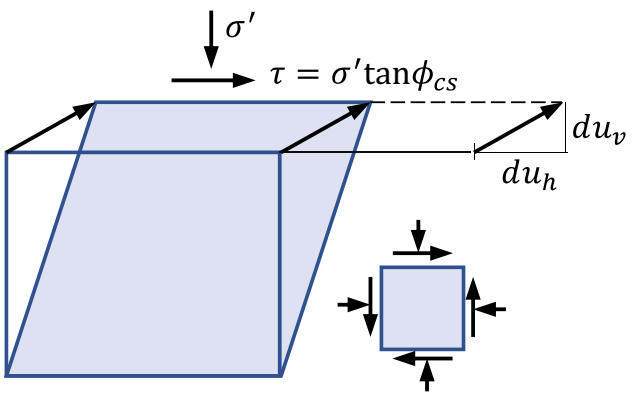

Fig. 1 Dilation of soil in a shear box

It was assumed that all elastic stored energy is negligible and that practically all the work done by the internal forces is dissipated (i.e., $\dot{W} = \Phi$) and the frictional dissipation is

$$\Phi = \sigma' \tan \phi_{cs} \mathrm{d}u_h \tag{7}$$

This hypothesis assumed that ϕ_{cs} is the mobilized friction angle ϕ_{cv} when the vertical deformation becomes steady state. By equating Eqs. (6) and (7), we may write the following stress–dilatancy relationship.

$$D = -\frac{\mathrm{d}u_v}{\mathrm{d}u_h} = \tan \phi_{cv} - \frac{\tau}{\sigma'} \tag{8}$$

We retrieve Taylor's decomposition of shearing strength of sands into pure "frictional resistance among grains" and a resistance due to "interlocking dilation" of grains. This interpretation is an attempt for a plausible micromechanical interpretation of the strength of sand. In Taylor's dilatancy equation, only the frictional dissipation term was considered.

A similar approach is used in the critical state (or Cam Clay) model [5, 24, 25, 41, 45] by assuming that the plastic part of the applied work is equal to the frictional dissipation.

$$\dot{W}^p = \Phi \tag{9}$$

Consider an assembly of grains undergoing plastic dilatant volumetric strain $\mathrm{d}\varepsilon_v^p$ and shear strain $\mathrm{d}\varepsilon_q^p$ when a set of mean effective stress p' and shear stress q are applied. The plastic work is defined by $\dot{W}^p = q\mathrm{d}\varepsilon_q^p + p'\mathrm{d}\varepsilon_v^p$, and the frictional dissipation function is given by $\Phi = p'M\mathrm{d}\varepsilon_q^p$ where M is the slope of critical state line in $p' - q$ plane. Assuming that $\dot{W}^p$ is solely equal to the frictional dissipation, then

$$q\mathrm{d}\varepsilon_q^p + p'\mathrm{d}\varepsilon_v^p = Mp\mathrm{d}\varepsilon_q^p \tag{10}$$

where for triaxial condition, $p' = \left(\sigma_1' + 2\sigma_3'\right)/3$, $q = \sigma_1 - \sigma_3$, $\varepsilon_q = \varepsilon_1 - \varepsilon_v/3$. The superscript '$p$' stands for plastic. It is noted that the applied work expression in Eq. (10) does not consider the case of non-coaxially between the principal stress and principal strain rate directions, which is an elusive feature that influences for the dilatancy behavior of sand [17, 53]. The corresponding stress–dilatancy relationship is expressed as:

$$\frac{\mathrm{d}\varepsilon_v^p}{\mathrm{d}\varepsilon_q^p} = \frac{q}{p'} - M \tag{11}$$

This equation has been applied to several constitutive models. However, this equation generally over predicts the dilatancy for dense sand. To avoid this shortcoming, Nova [36] applied a correction factor c to the dilatancy (i.e., $c\frac{\mathrm{d}\varepsilon_v^p}{\mathrm{d}\varepsilon_q^p}$). The value of c appears to be soil type dependent,

which is found to be 0.5 for Ottawa sand [53], and 0.63–0.75 for Erksak sand [3]. Instead of being a constant, the value of c is assumed to be a function dependent on M, e.g. $c = c_0 M$ [30] and $c = 1 - M/3$ [48].

Another class of dilatancy equation was proposed by Rowe [43], Newland and Alley [33], and de Joselin de Jong [27], Wan and Guo [57], etc. Although Rowe's dilatancy equation was not derived directly from thermodynamics, it was shown by Guo [15] that Rowe's dilatancy equation can be recovered from the same assumption that the applied work is solely equal to the frictional dissipation.

Considering an assembly of grains deformed in a triaxial condition, Rowe's stress-dilatancy equation couples the mobilized friction angle ϕ_m to the dilation angle ψ in the following convenient form

$$\sin\psi = \frac{\sin\phi_m - \sin\phi_f}{1 - \sin\phi_m \sin\phi_f} \tag{12}$$

where ϕ_f is a material parameter, which changes with initial void ratio and stress level. For convenience, ϕ_f is commonly assumed to be equal to ϕ_{cv}. The mobilized friction angle ϕ_m and the dilation angle ψ are defined by

$$\sin\psi = \frac{-(\mathrm{d}\varepsilon_v/\mathrm{d}\varepsilon_1)}{2 - (\mathrm{d}\varepsilon_v/\mathrm{d}\varepsilon_1)};\ \sin\phi_m = \frac{\sigma_{1-}\sigma_3}{\sigma_1 + \sigma_3} \tag{13}$$

A formal derivation of Eq. (12) from Eq. (13) and its application to triaxial compression and plane strain conditions can be found in the literature [44, 54].

Correction factors for the dilation angle are also found in the literature. The results of DEM simulations performed by Alonso-Marroquin et al. [2] and Kruyt and Rothenburg [28] showed that, irrespective of the inter-particle friction and particle shape, $\sin\psi$ in Eq. (12) can be replaced by $c\sin\psi$ with c = 0.58–0.62. Powrie et al. [39] also reported that c = 0.5.

Another correction factor is suggested to modify the value ϕ_f by the consideration that void ratio is a factor influencing the dilatancy behavior of sand [57], given by

$$\sin\phi_f = (e/e_{cr})^{\alpha}\sin\phi_{cv} \tag{14}$$

where α is a constant, e and e_{cr} are the current void ratio and the critical void ratio, respectively. For the same reasoning to include void ratio as variable, Li and Dafalias [30] applied a correction factor to the value of M by $M \cdot \exp(m(e - e_{cr}))$. However, in the study by Been and Jefferies [3] on the dilatancy behavior of very loose sand, they stated that it is unclear that this correction factor, as a function of void ratios, is an appropriate choice.

The above mentioned stress–dilatancy relationships are based on the hypothesis that plastic work $\dot{W}^p$ consists only frictional dissipation as shown in Eq. (9). Recently, observed from acoustic experiments, it has been found that plastic energy can be produced by deformation mechanisms other than friction between particles [31, 47]. Thus, it is necessary to account for the Helmholtz free energy in order to correctly model the stress-dilatancy behavior. A couple of models have considered the Helmholtz free energy Ψ^p (see Eq. 5) in the energy equation for deriving the stress–dilatancy relationship, notably by Jefferies [25], and Collins and Kelly [10]. They demonstrated that the energy equation fundamentally linked to the dilatancy behavior of sand.

In the following, the stress–dilatancy relationships derived by Jefferies [25], and Collins and Kelly [10] will be briefly described and compared with the experimental results in a later section. Based on experimental results, we propose new formulations for the equation of energy conservation. The resulted stress–dilatancy relationship is then compared with other models and with the measured results for Silica sand [13], Ottawa sand [16], and Nevada sand [35]. Discussion is given on the process of calibration of parameters based on measurable physical properties, and on the influence factors of soil density and confining stress.

2 Existing models considering plastic Helmholtz free energy

At the micro or contact scale, the major dissipative mechanism for cohesionless systems is friction, with plastic slip as the internal variable (see, for example, Tordesillas and Walsh [51]). There is, however, compelling evidence from DEM simulations indicating that dissipation in friction does not equal to the applied plastic work in a quasi-statically loaded cohesionless assembly [28, 42, 55]. Various studies have shown that, for constitutive models in which friction serves as the sole source of plastic work, the dilation is not properly accounted and could over predict the material stability [1, 6, 32, 51]. Thus, besides the frictional dissipation Φ, an additional term of plastic Helmholtz free energy $\dot{\Psi}^p$ should be added.

$$q\mathrm{d}\varepsilon_q^p + p'\mathrm{d}\varepsilon_v^p = \Phi + \dot{\Psi}^p \tag{15}$$

To consider the term of plastic Helmholtz free energy, a form of energy equation was proposed by Collins and Kelly [10], in which the frictional dissipation is similar to that of the modified Cam Clay model.

$$\Phi = \frac{1}{2}p_c\sqrt{(\mathrm{d}\varepsilon_v^p)^2 + (M\mathrm{d}\varepsilon_q^p)^2} \tag{16}$$

And the Helmholtz free energy is assumed to be dependent on plastic volume strain increment [7]

$$\dot{\Psi}^p = \frac{1}{2} p_c \mathrm{d}\varepsilon_v^p \tag{17}$$

where the stress parameter p_c is the mean normal consolidation pressure, calculated from an elliptical yield locus given by

$$p_c = p' \frac{M^2 + (q/p')^2}{M^2} \tag{18}$$

Thus, the energy equation is written as

$$q\mathrm{d}\varepsilon_q^p + p'\mathrm{d}\varepsilon_v^p = \frac{1}{2} p_c \sqrt{(\mathrm{d}\varepsilon_v^p)^2 + (M\mathrm{d}\varepsilon_q^p)^2} + \frac{1}{2} p_c \mathrm{d}\varepsilon_v^p \tag{19}$$

Collins and Hilder [8] showed that the form of energy equation has a fundamental influence on constitutive equations such as yield function [11]. From Eq. (19), Collins and Kelly [54] derived the resultant stress–dilatancy relationship, which was found to be identical to that of modified Cam Clay model [40].

$$\frac{\mathrm{d}\varepsilon_v^p}{\mathrm{d}\varepsilon_q^p} = \left(M^2 - (q/p')^2\right)/(2q/p') \tag{20}$$

Another energy equation that contains a Helmholtz free energy term was suggested by Jefferies [25] in the following form

$$q\mathrm{d}\varepsilon_q^p + p'\mathrm{d}\varepsilon_v^p = Mp'\mathrm{d}\varepsilon_q^p + Np'\mathrm{d}\varepsilon_v^p \tag{21}$$

The term of Helmholtz free energy is similar to that proposed by Collins and Kelly [10] in Eq. (17). Jefferies showed that, from Eq. (21), the stress–dilatancy relationship can be derived as:

$$\frac{\mathrm{d}\varepsilon_v^p}{\mathrm{d}\varepsilon_q^p} = \frac{1}{1-N}(M - q/p') \tag{22}$$

The parameter N is related to the correction factor c(i.e., $c = 1 - N$) proposed by Nova [36]. Jefferies suggested that commonly, $N = 0.25$, implying that the dissipation energy is not equal to the externally applied work. The N value significantly alter the stress-dilatancy characteristics.

These results demonstrated that the stress–dilatancy relationship is directly influenced not only by the form of frictional dissipation function Φ but also by the form of Helmholtz free energy $\dot{\Psi}^p$. In the following, we will investigate the appropriate forms of the energy equations for three types of sand (i.e. Silica sand [13], Ottawa sand [16], and Nevada sand [35]) and their implications to stress–dilatancy relationship.

3 Experimental results

3.1 Silica sand and its stress–strain results

Drained triaxial test results of Pasabahce silica sand (herein referred to as silica sand) is selected for this study [13]. Samples were prepared by the following seven grades of "uniform" sands: No.16–No.18, No.18–No.30, No.30–No.50, No.50–No.80, No.80–No.100, No.100–No.120, No.120–No.200. Each uniform sand is named by the upper and the lower sieve numbers. The particle sizes and specific gravities of these seven uniform sands are listed in Table 1. The shapes of the sand grains are mostly sub-angular. The minimum and the maximum void ratios of samples are tabulated in Table 1.

Samples were prepared at nearly the same relative density of around 95%. The drained triaxial compression tests for each sample were performed under three different effective confining stresses of 100 kPa, 200 kPa, and 400 kPa. Particle breakage was not observed in all tests.

Figure 2 shows stress ratio $\eta = q/p'$ (where $q = \sigma_1 - \sigma_3$) and volumetric strain (ε_v) versus deviatoric strain (ε_q) relationships for the 7 uniform silica sands under three different confining stresses (100, 200, 400 kPa). As shown in Fig. 2, all samples after peak exhibit softening behavior in the stress–strain curves and exhibit dilative behavior in the volumetric strain curves. Following the initial slight contraction at a small axial strain, dilation then commences. The dilation continues during shearing until the deviatoric stress q mobilizes to the peak value. After the peak deviatoric stress, the stress decreases and approaches to a stable value (the critical state).

Kinks can be found in the stress ratio vs strain curves for the samples with particle size from 0.10 to 0.16 mm. For these samples, shear band were observed at end of test. Comparing to samples with larger particle sizes, the

Table 1 Properties of the uniform silica sands of seven different particle sizes

Uniform sand*	d_{50} (mm)	e_{max}	e_{min}	Roundness	G_s
#16–#18	1.086	0.901	0.632	0.36	2.624
#18–#30	0.775	0.907	0.64	0.35	2.625
#30–#50	0.424	0.999	0.698	0.26	2.64
#50–#80	0.232	1.102	0.786	0.17	2.646
#80–#100	0.164	1.128	0.768	0.19	2.654
#100–#120	0.137	1.108	0.778	0.18	2.652
#120–#200	0.096	1.099	0.717	0.23	2.654

*The uniform silica sand is artificially graded using two adjacent sieves. # No.– # No. is the upper and the lower sieve numbers, respectively, for a uniform sand

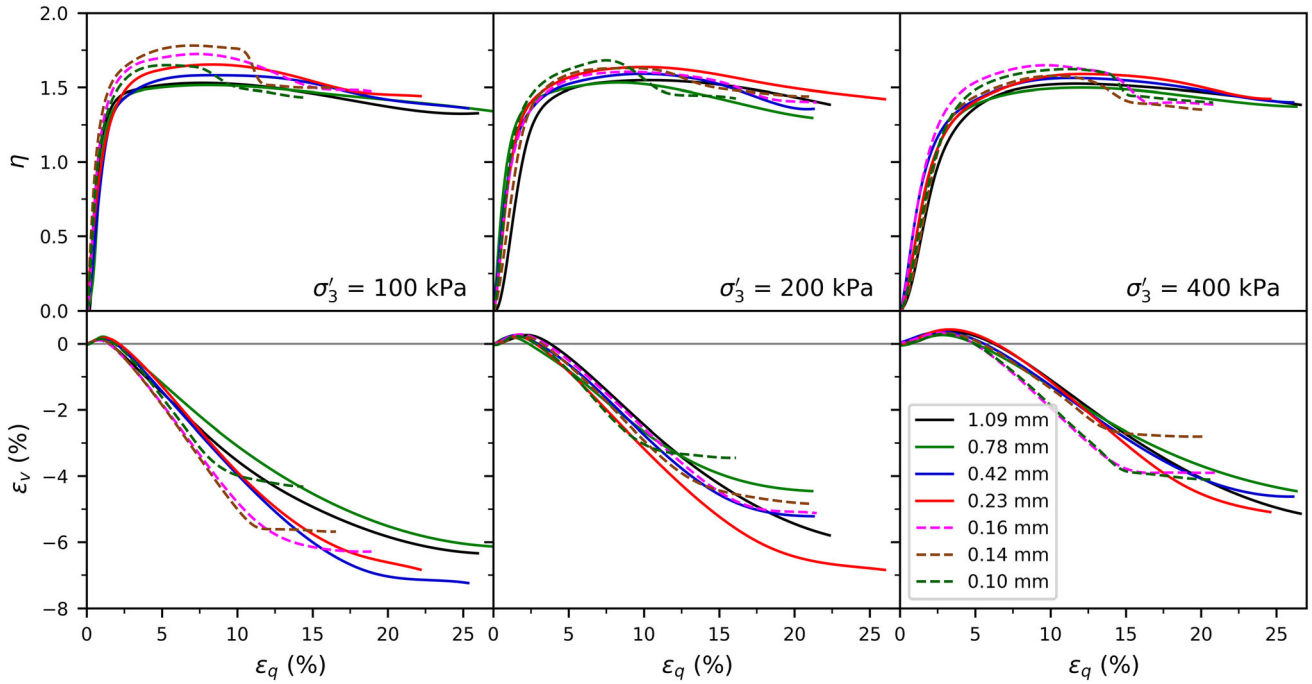

Fig. 2 Relationships between stress ratio $\eta = q/p'$ (where $q = \sigma_1 - \sigma_3$) and volumetric strain (ε_v) versus deviatoric strain (ε_q) for the seven uniform silica sands under three different confining stresses

smaller particle samples are likely to form shear band, which has been explained from the viewpoint of particle column buckling in the recently published paper [13].

3.2 Ottawa sand and its stress–strain results

Drained triaxial test results of Ottawa sand are also selected for this study [16]. Particles of Ottawa sand are rounded in shape. Its $e_{\max}$ and $e_{\min}$ are 0.811 and 0.503, respectively. The mean particle size of Ottawa sand D_{50} = 0.376 mm. Samples were prepared at three different initial void ratios (e_0 = 0.584, 0.711, and 0.773) and sheared at an effective confining pressure of 100 kPa. The experimental results of Ottawa sand are shown in Fig. 3. In these tests, particle breakage and shear band were not reported.

3.3 Nevada loose sand and its stress–strain results

Drained triaxial test results of Nevada sand are also selected for this study [35]. Particles of Nevada sand are subrounded in shape. Its $e_{\max}$ and $e_{\min}$ are 0.856 and 0.548, respectively. The mean particle size D_{50} is 0.144 mm. Samples were prepared at initial void ratios e_0 = 0.905 $\sim$ 0.936 and sheared at an effective confining pressure of 10 kPa $\sim$ 200 kPa. The experimental results of Nevada sand are shown in Fig. 4.

4 Energy equation

4.1 Elastic and plastic strain

According to the elastoplastic theory, the total strain increment can be decomposed into plastic strain and elastic strain increments. The elastic shear modulus of an assembly of particles is assumed to be computed by the following equations [20]:

$$G = G_0 p_a \frac{(c_g - e)^2}{1+e}\left(\frac{p'}{p_a}\right)^n \tag{23a}$$

where the value $n = 0.4$, $p_a = 101.3$ kPa. The value c_g = 2.17 for round sand and 2.79 for angular sand. G_0 is 160 for Silica sand and Nevada sand, and 300 for Ottawa sand. e is current void ratio which can be calculated from initial void ratio e_0 and total volumetric strain ε_v, i.e. $e = e_0 - \varepsilon_v \cdot (1 + e_0)$. The elastic bulk modulus K can be computed by

$$K = G\frac{2(1+v)}{3(1-2v)} \tag{23b}$$

In this study, the Poisson's ratio v is assumed to be 0.2. The elastic shear and volume strains are computed by

$$\varepsilon_v^e = p'/K;\ \varepsilon_q^e = q/3G \tag{24}$$

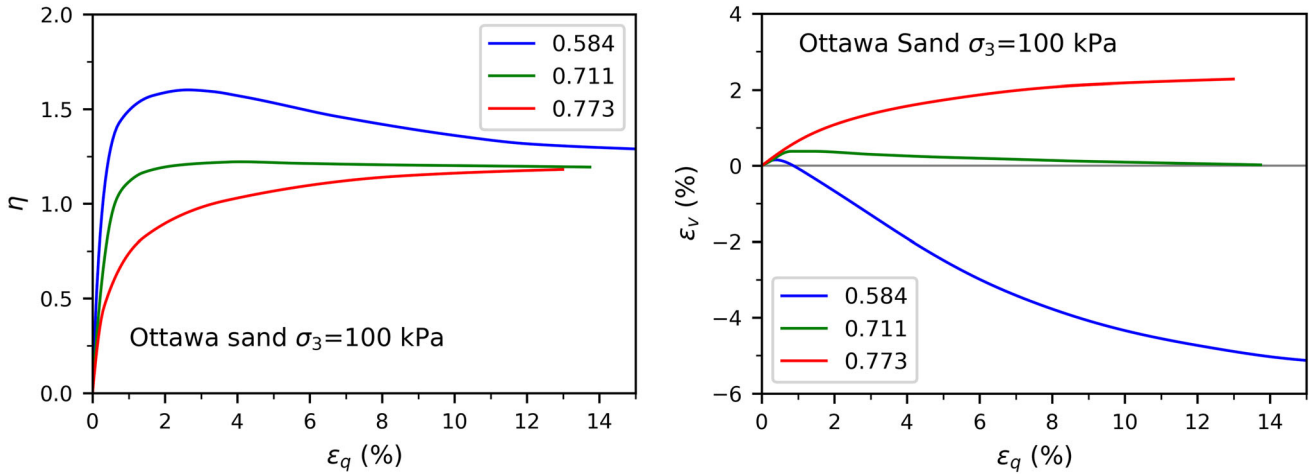

Fig. 3 Relationships between stress ratio η and volumetric strain (ε_v) versus axial strain (ε_a) for Ottawa sand with three different initial densities

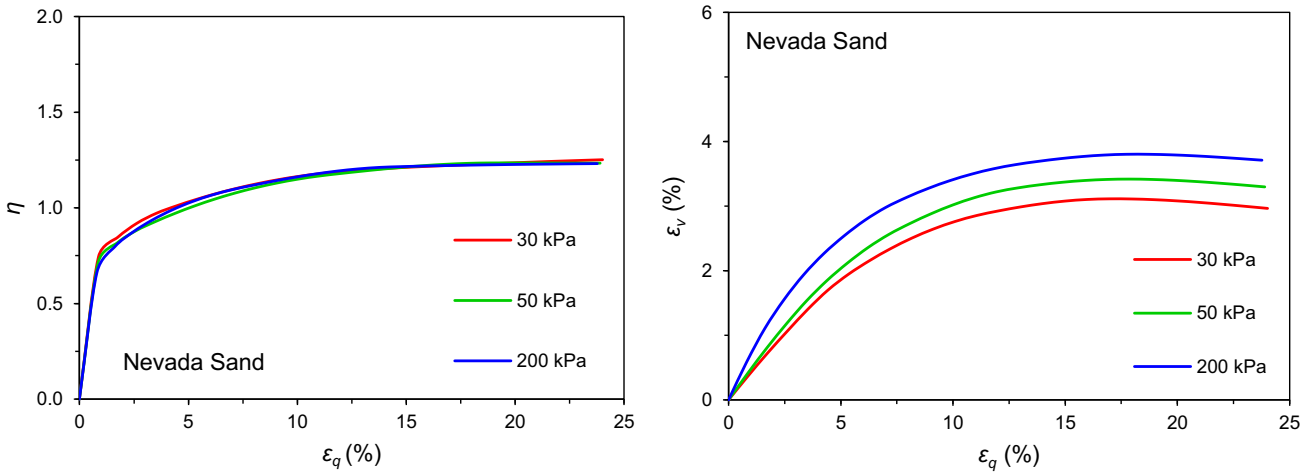

Fig. 4 Relationships between stress ratio η and volumetric strain (ε_v) versus axial strain (ε_a) for Nevada sand with different confining stresses

It is noted that there is a coupling effect between the elastic and plastic strains due to the evolution of modulus with void ratio (i.e., plastic volume strain) [9, 14].

The total derivative of Eq. (24) yields

$$\mathrm{d}\varepsilon_v^e = \frac{\mathrm{d}p'}{K} - \frac{p'}{K^2}\left(\frac{\partial K}{\partial p'}\mathrm{d}p' - \frac{\partial K}{\partial e}\mathrm{d}e\right) \tag{25a}$$

$$\mathrm{d}\varepsilon_q^e = \frac{\mathrm{d}q}{3G} - \frac{q}{3G^2}\left(\frac{\partial G}{\partial p'}\mathrm{d}p' - \frac{\partial G}{\partial e}\mathrm{d}e\right) \tag{25b}$$

The second terms on the right hand of Eqs. (25a and 25b) are the elastic component coupled with the plastic strain, which is not exist in the conventional elastoplastic model. The plastic strain increments, $\mathrm{d}\varepsilon_v^p$ and $\mathrm{d}\varepsilon_q^p$ can be obtained by subtracting the calculated the elastic strain increment from the measured total strain increment.

For a drained triaxial test on sand, the elastic strain increment is very small compared with plastic strain increment. And only a portion of elastic strain is coupled with plastic strain. Therefore, the coupling effect can be ignored in estimating the plastic work, frictional dissipation, and plastic Helmholtz free energy, as evaluated in Appendix A.

4.2 Imbalance of energy equation

In general, the frictional dissipation is a function of plastic strain increment $\Phi\left(\mathrm{d}\varepsilon_v^p, \mathrm{d}\varepsilon_q^p\right)$. However, the frictional dissipation energy of Taylor-Cam Clay type is only a function of shear strain (i.e.$Mp'\mathrm{d}\varepsilon_q^p$, see Eq. 10). In this restricted context, the form in Eq. (10) is not ideal because it does not consider the frictional dissipation due to plastic volume strain [10]. On the other hand, the frictional energy of Taylor-Cam Clay type has been widely used in various constitutive models [12, 24, 36, 58] and the hypothesis has been supported by several studies of DEM simulations [18, 28], in which, the frictional dissipations calculated

from inter-particle contacts were found to be very close to that computed from the Taylor-Cam Clay model. Thus, in the first approximation, we use the expression $\Phi = Mp'\mathrm{d}\varepsilon_q^p$ for the frictional dissipation energy.

To compare the magnitudes of $\dot{W}^p$ and Φ, we plot the externally applied plastic work $\dot{W}^p$ and the frictional energy dissipation Φ in Fig. 5 for dense Silica sand (#30–#50, see Table 1) with three different confining stresses, in Fig. 6 for Ottawa sand with three different initial densities, and in Fig. 7 for loose Nevada sand with three different confining stresses. Note that the dissipation energy is a function of plastic shear strain rate. The plastic shear strain rate is not zero at the point of zero shear strain. Therefore, both the calculated dissipation energy and total work are nonzero at zero strain.

It is noted that for all cases in Figs. 5, 6 and 7, the plastic applied work is not equal to frictional dissipation, i.e., $\dot{W}^p \neq \Phi$. For silica sand, the difference between the two values seems to be proportional to confining stress. For Ottawa sand, the difference between these two values are significantly larger for dense sand and negligibly small for very loose sand. Similarly, the difference is insignificant for loose Nevada sand.

The difference between $\dot{W}^p$ and Φ may be caused by two reasons: (1) the Helmholtz free energy should be considered in additional to the frictional dissipation energy, as indicated in the first law of thermodynamics (see Eq. 3) and (2)the expression of the frictional energy estimated by $Mp'\mathrm{d}\varepsilon_q^p$ could be incorrect and overestimated. These two possible causes are discussed below.

4.3 Consideration of Helmholtz free energy

According to thermodynamics (see Eq. 3), the term of Helmholtz free energy $\dot{\Psi}^p$ is generally required to balance the externally applied plastic work. Thus, the energy equation of Taylor-Cam Clay type becomes

$$\underbrace{q\mathrm{d}\varepsilon_q^p + p'\mathrm{d}\varepsilon_v^p}_{\dot{W}^p} \equiv \underbrace{Mp'\mathrm{d}\varepsilon_q^p}_{\Phi} + \dot{\Psi}^p \tag{26}$$

The dissipation energy is a quantity that must always be positive. However, Helmholtz free energy $\dot{\Psi}^p$ can be either

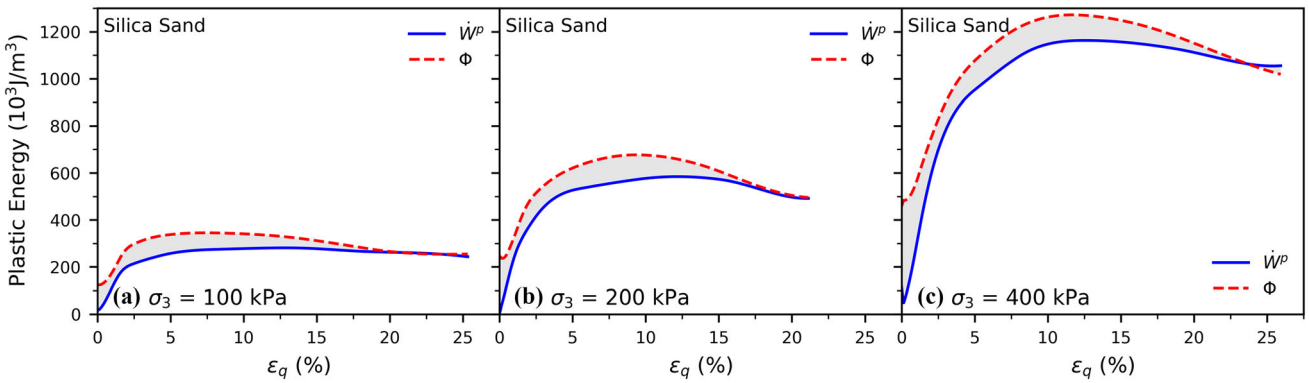

Fig. 5 Plastic work and frictional dissipation energy versus shear strain for dense Silica sands under three different confining pressures (100 kPa, 200 kPa, and 400 kPa). The calculated plastic energy is normalized per unit axial strain under the triaxial loading condition

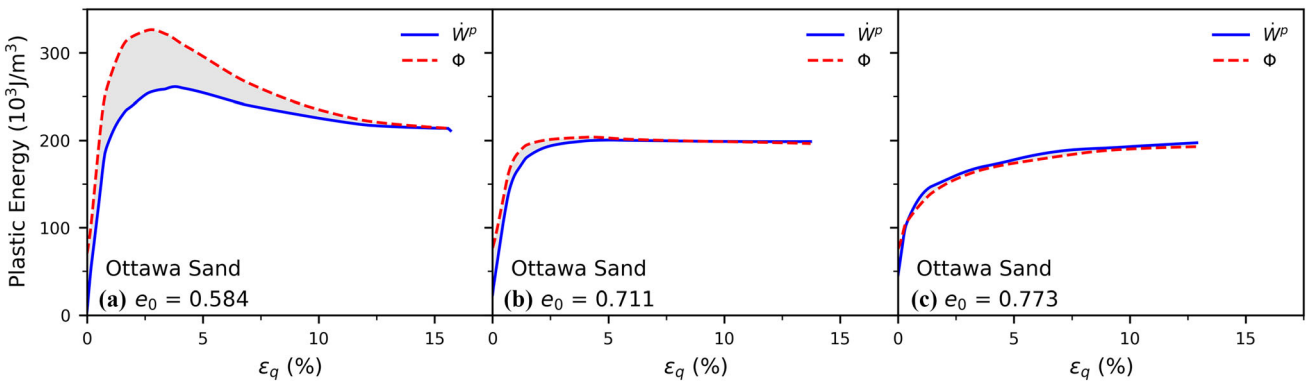

Fig. 6 Plastic work and frictional dissipation energy versus shear strain for Ottawa sands under three different initial densities (dense, loose and very loose). The calculated plastic energy is normalized per unit axial strain under the triaxial loading condition

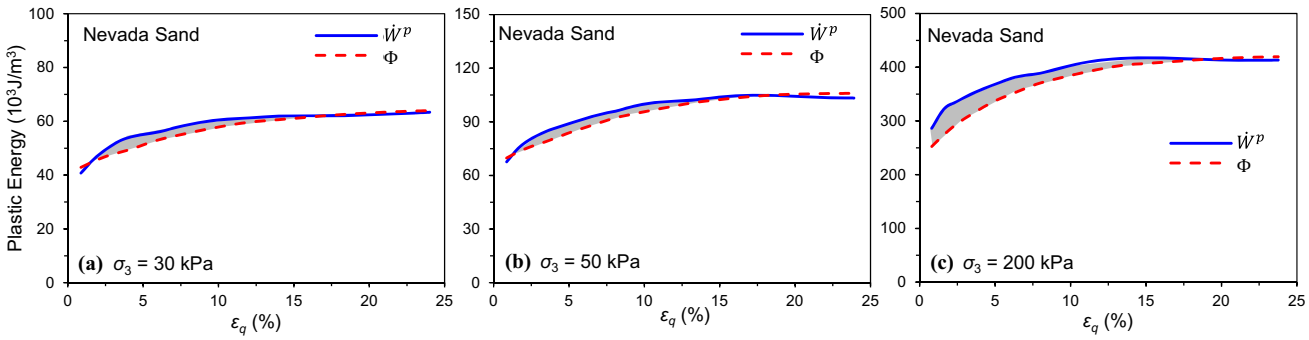

Fig. 7 Plastic work and frictional dissipation energy versus shear strain for loose Nevada sands under three different confining pressures (30 kPa, 50 kPa, and 200 kPa). The calculated plastic energy is normalized per unit axial strain under the triaxial loading condition

positive or negative. Figures 5, 6 and 7 show, for loose sand, $\dot{W}^p > \Phi$, thus according to energy balance, the free energy $\dot{\Psi}^p = \dot{W}^p - \Phi$ is positive, which means that part of the applied plastic work is dissipated, and the other part (i.e., $\dot{\Psi}^p$) is stored into the internal energy of particle system.

On the other hand, $\dot{W}^p < \Phi$ for dense sand, thus the free energy $\dot{\Psi}^p = \dot{W}^p - \Phi$ is negative, which means that not only all applied plastic work is dissipated, but also additional plastic work (i.e., $\dot{\Psi}^p$) is dissipated. The additional part is extracted from the available internal energy of the particle system.

The Helmholtz free energy $\dot{\Psi}^p$ is also term as free energy because it can be either stored or extracted from the system. It is noted that whether the free energy is positive or negative is associated with the shear induced volume contraction or dilation in a particle system.

In a triaxial test for a loose specimen, volume contraction is caused by rearrange of particles, which leads to a collapsing of voids and an increase of internal energy of the system. In contrast, for a dense specimen, dilation of specimen is caused mainly by buckling of force chains [13, 37, 50, 60] and the associated growth of surrounding voids [23, 37, 38]. Thus, the mechanism of buckling of force chains characteristically involves the collective release of stored energy.

Figures 5, 6 and 7 show that the difference between applied work and frictional dissipation energy (i.e., the Helmholtz free energy $\dot{\Psi}^p$) is caused by volume contraction or dilation in a particle system. Thus, it is reasonable to assume that the Helmholtz free energy is a function of plastic volume strain increment, i.e.$\dot{\Psi}^p = Np'\mathrm{d}\varepsilon_v^p$. Thus, Eq. (26) becomes:

$$q\mathrm{d}\varepsilon_q^p + p'\mathrm{d}\varepsilon_v^p = Mp'\mathrm{d}\varepsilon_q^p + Np'\mathrm{d}\varepsilon_v^p \tag{27}$$

Let $D = -\mathrm{d}\varepsilon_v^p/\mathrm{d}\varepsilon_q^p$, which is positive for dilation, then the energy Eq. (27) can lead to a stress–dilatancy relationship in the form:

$$\eta^{(2)} = M + (1-N)D \tag{28}$$

where $\eta^{(2)} = q/p'$ represents the stress ratio calculated from Eq. (28). When $N = 0$, Eq. (28) reduces to the classic form of Taylor-Cam Clay type (see Eq. 11)

$$\eta^{(1)} = M + D \tag{29}$$

where $\eta^{(1)} = q/p'$ represents the stress ratio calculated from the classic Taylor-Cam Clay.

The solid line in Fig. 8 shows a typical measured stress–strain curve for dense sand, which has three characteristic states—namely, the phase transformation state (the onset point where the volumetric-strain increment is zero at $\eta = \eta_d$), the peak sate (where the stress peaks at $\eta = \eta_{\max}$), and the critical state at large shear strain (where the volumetric-strain increment and stress increment are both zero at $\eta = M$). The maximum dilatancy $D_{\max}$ is defined as the

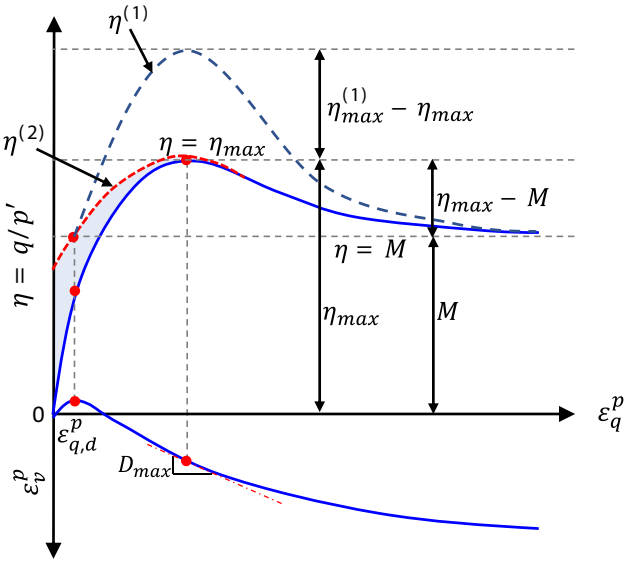

Fig. 8 The measure stress ratio η compared with those calculated from Eqs. (28) and (29)

maximum ratio of $d\varepsilon_v^p/d\varepsilon_q^p$, which is corresponding to the peak state.

The blue dashed line $\eta^{(1)}$ represents the curve calculated from Eq. (29) without consideration of the term of Helmholtz free energy. The red dashed line $\eta^{(2)}$ represents the curve calculated from Eq. (28) with consideration of the term of Helmholtz free energy, which fits better to the measured curve (in solid line).

At peak stress state, Eq. (29) becomes

$$\eta_{\max}^{(1)} = M + D_{\max} \tag{30}$$

And Eq. (28) becomes

$$\eta_{\max}^{(2)} = M + (1 - N)D_{\max} \tag{31}$$

We want to match the peak stress ratio $\eta_{\max}^{(2)}$ with the measured peak stress ratio $\eta_{\max}$. Substituting $\eta_{\max}^{(2)} = \eta_{\max}$ into Eq. (31), it leads to

$$N = 1 - (\eta_{\max} - M)/D_{\max} \tag{32}$$

The value of N can be obtained from Eq. (32) based on the measured values of $\eta_{\max}$ and $D_{\max}$.

Equation (32) can be used to determine the value of N for most densities of sand, in which peak state exists in their stress–strain curves. However, for cases of very loose sand, peak is not revealed. The value of N can be determined by try and error for best fitting the experimental data.

Using Eq. (32), the calibrated N values for silica sand are 0.49 for the confining stress of 100 kPa, 0.41 for the confining stress of 200 kPa, and 0.31 for the confining stress of 400 kPa. The calibrated N values for Ottawa sand are 0.35 for dense sand, 0.38 for loose sand, and 0.22 for very loose sand. The calibrated N values for Nevada loose sand are 0.607 for all confining stresses. The measured values M = 1.357 for Silica sand, M = 1.183 for Ottawa sand, and M = 1.23 for Nevada sand.

To evaluate the calibrated values of N for the Helmholtz free energy term, we compare the calculated energy $(\Phi + \dot{\Psi}^p)$ from Eq. (27) with the measured $\dot{W}^p$ for Silica sand plotted in Fig. 9. We also compare the energy curves for Ottawa sand plotted in Fig. 10, and for Nevada sand plotted in Fig. 11.

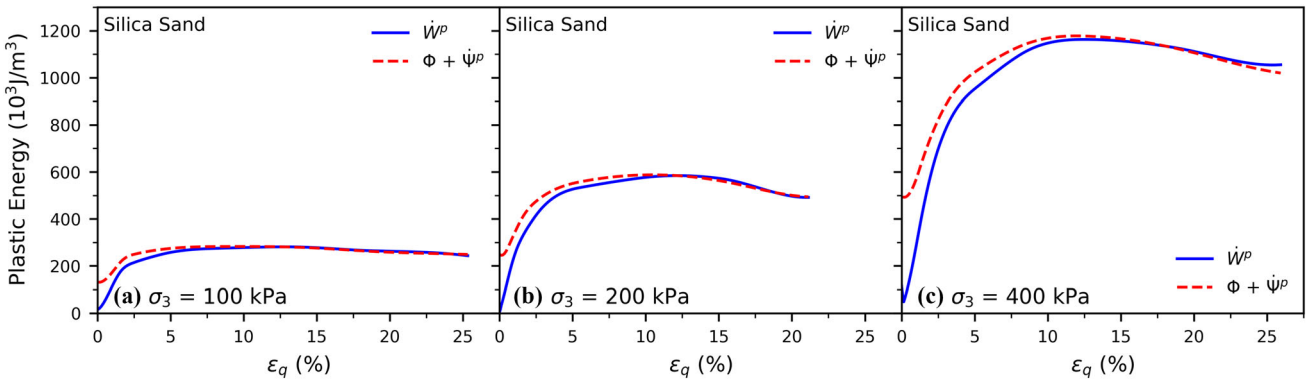

Fig. 9 Work $\dot{W}^p$ and plastic energy $(\Phi + \dot{\Psi}^p)$ versus shear strain for Silica sand under three different confining stresses. The calculated plastic energy is normalized per unit axial strain under the triaxial loading condition

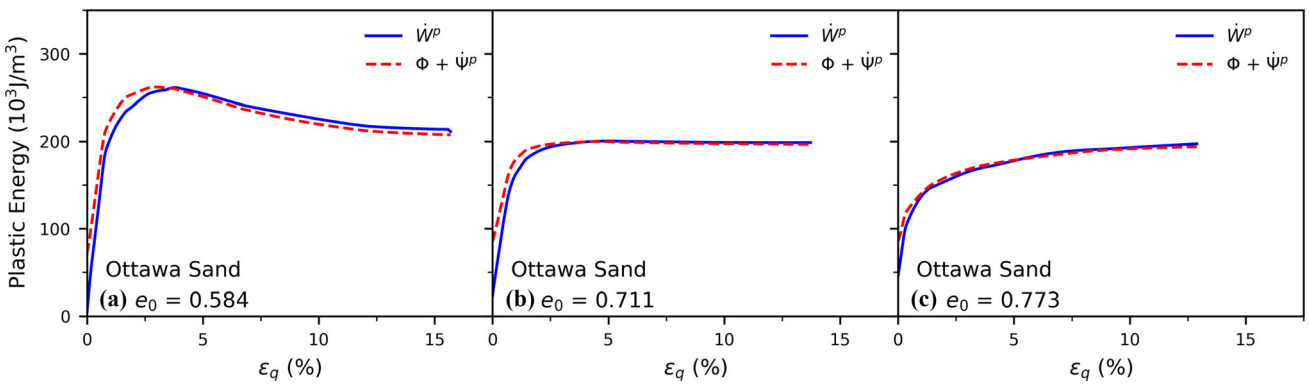

Fig. 10 Work $\dot{W}^p$ and plastic energy $(\Phi + \dot{\Psi}^p)$ versus shear strain for Ottawa sand under three different initial densities. The calculated plastic energy is normalized per unit axial strain under the triaxial loading condition

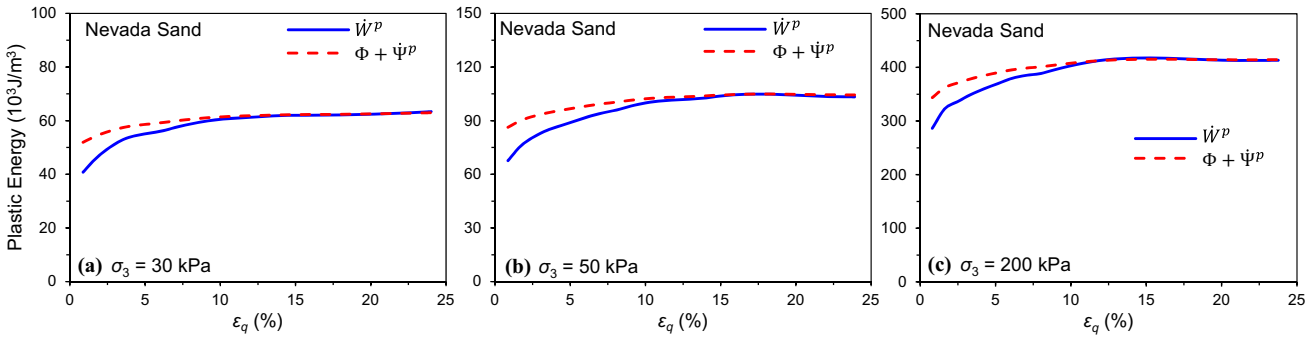

Fig. 11 Work $\dot{W}^p$ and plastic energy $(\Phi + \dot{\Psi}^p)$ versus shear strain for Nevada sand under three different confining stresses. The calculated plastic energy is normalized per unit axial strain under the triaxial loading condition

Figures 9, 10 and 11 show that, with the consideration of $\dot{\Psi}^p$, agreements between the two energy curves are largely improved than those shown in Figs. 5, 6 and 7 computed without consideration of $\dot{\Psi}^p$.

It is noted that the value N can be determined from two readily measurable parameters $\eta_{\max}$ and $D_{\max}$ as shown in Eq. (32). The physical meaning of N represents the magnitude of shear resistance $(\eta_{\max} - M)$ that can be produced from the dilation of grains $D_{\max}$. The N value is likely to be associated with the shape and surface roughness of particles. Figure 12 shows the measured value of $(\eta_{\max} - M)$ versus $D_{\max}$ for Silica sand for seven different particles sizes (Table 1) and for Ottawa sand. For each type of soil, the relationship can be approximated by a linear line. The slope of the line is $(1 - N)$. It shows that the average value of N is 0.37 for Erksak sand [3] and is 0.5 for Silica sand, compared to $N = 0$ for the Taylor-Cam Clay model.

Equation (31) is comparable with the Bolton's dilatancy equation [4],

$$\phi_p - \phi_{cv} = b\psi_p \tag{33}$$

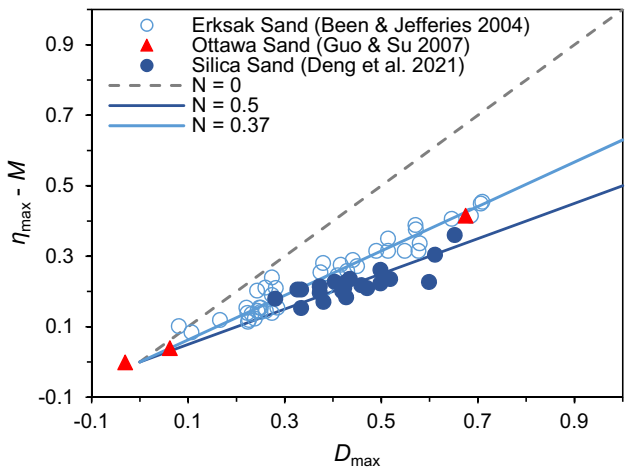

Fig. 12 The meaning of parameter N

where ψ_p is the angle of dilation at peak state, ϕ_p and ϕ_{cv} are the friction angles of friction at peak state and at critical state, respectively. It is noted that the physical meaning of b is equivalent to that of $(1 - N)$. In Fig. 12, the value of N can also be determined from the b coefficient of the Bolton's dilatancy equation.

4.4 Additional imbalance due to the incorrect expression of frictional dissipation energy

Although Figs. 9, 10 and 11 show that the balance of energy equation is improved with the term of Helmholtz free energy, the imbalance are still noticeable between the applied work and the sum of dissipation energy Φ and Helmholtz free energy $\dot{\Psi}^p$. The imbalance of energy equation is not negligible for the region of small shear strain, particularly prior to peak stress state for the dense sand. Therefore, an additional energy δE is needed to balance the equation.

$$q\mathrm{d}\varepsilon_q^p + p'\mathrm{d}\varepsilon_v^p = Mp'\mathrm{d}\varepsilon_q^p + Np'\mathrm{d}\varepsilon_v^p + \delta E \tag{34}$$

Figures 9, 10, and 11 show that the energy δE is negative and is a function of plastic shear strain ε_q^p. This discrepancy is attributed to the overestimated frictional energy using the expression $Mp'\mathrm{d}\varepsilon_q^p$.

Let β be the ratio of δE to the frictional dissipation, i.e. $\beta\left(\varepsilon_q^p\right) = -\delta E/Mp'\mathrm{d}\varepsilon_q^p$, the energy Eq. (34) can be expressed by

$$q\mathrm{d}\varepsilon_q^p + p'\mathrm{d}\varepsilon_v^p = \left(1 - \beta\left(\varepsilon_q^p\right)\right)Mp'\mathrm{d}\varepsilon_q^p + Np'\mathrm{d}\varepsilon_v^p \tag{35}$$

In Eq. (35), the term of $\left(1 - \beta\left(\varepsilon_q^p\right)\right)Mp\mathrm{d}\varepsilon_q^p$ represents the frictional energy dissipation. Note that the energy δE is negative, thus $\beta\left(\varepsilon_q^p\right)$ is positive, which means a reduction of the estimated frictional energy. The function of $1 - \beta\left(\varepsilon_q^p\right)$ indicates that the value of frictional dissipation is

not a constant, but varies with the shear strain ε_q^p. This hypothesis is examined below.

The energy Eq. (35) leads to the following stress-dilatancy relationship,

$$\eta^{(3)} = \left(1 - \beta\left(\varepsilon_q^p\right)\right)M + (1 - N)D \tag{36}$$

where the function $\beta\left(\varepsilon_q^p\right)$ is represented by the shaded zone schematically shown in Fig. 13. $\eta^{(3)}$ represents the value of η calculated from Eq. (36). Since Eq. (36) is advocated so that $\eta^{(3)}$ best fits the measured curve, thus assuming $\eta^{(3)} = \eta$, and Eq. (36) can be expressed as

$$1 - \beta\left(\varepsilon_q^p\right) = (\eta - (1 - N)D)/M \tag{37}$$

Using Eq. (37) and experimental data,$1 - \beta\left(\varepsilon_q^p\right)$ is plotted in Fig. 14a for Silica sand, Fig. 14b for Ottawa sand, and Fig. 14c for Nevada sand, which show that the shape of $\beta\left(\varepsilon_q^p\right)$ resembles an exponential curve, given by

$$\beta\left(\varepsilon_q^p\right) = b' \cdot \exp\left(-m\varepsilon_q^p\right) \tag{38}$$

At the initial state $\eta = 0$, $\varepsilon_q^p = 0$, and $D = D_0$. From Eqs. (37) and (38), we obtain

$$b' = 1 + (1 - N)D_0/M \tag{39}$$

The dilatancy D_0 at initial state can be obtained from experiments, which is negative (i.e., contractive). Thus, the value b', calculated from Eq. (39), is less than 1. The value of b' is 0.83 for Silica sand, 0.73 for Ottawa sand, and 0.65 for Nevada sand.

For dense sand, the value m in Eq. (38) can be calibrated from the measures stress ratio η_d at the onset of dilation ($D = 0$), as shown in Fig. 13. At the onset of dilation $\eta = \eta_d$ and $\varepsilon_q^p = \varepsilon_{q,d}^p$, from Eq. (37) and Eq. (38), we obtain

$$1 - \eta_d/M = b' \cdot \exp\left(-m\varepsilon_{q,d}^p\right) \tag{40}$$

For cases of loose sand, in which dilation is not revealed, the value of m can be determined by try and error for best fitting Fig. 14 plotted from experimental data.

With Eq. (40), the m value calibrated for Silica sand (#30–#50) is 0.95 for 100 kPa, 0.95 for 200 kPa, and 0.70 for 400 kPa. The m value for Ottawa sand is 5 for dense sand, 3 for loose sand, and 5 for very loose sand. The m value for Nevada sand is 0.35 for confining stresses 30, 150, 200 kPa. It is noted that the value of b' can be regarded as 1, which is insensitive to the fitted results.

Note that the term of $\left(1 - \beta\left(\varepsilon_q^p\right)\right)Mp\mathrm{d}\varepsilon_q^p$ represents the frictional energy dissipation. The function of $1 - \beta\left(\varepsilon_q^p\right)$ in Fig. 14 indicates that the value of frictional dissipation is initially nearly zero, increases with the shear strain ε_q^p and approach to one near peak state. The dependency of shear strain is a reasonable hypothesis because frictional dissipation is induced from mobilization between contacts due to the relative motion between contacts via rolling and sliding. The amount of mobilized contacts depends on the level of shear deformation. Thus, frictional dissipation is influenced by the level of shear strain.

In the initial stage of shearing, the number of mobilized particle contacts is only a small portion of the total number of particles. The number of mobilized particle contacts increases with shear stress level. Figure 14 shows that the frictional energy, started from a small value, increases quickly in an exponential form, approaching to the value of $Mp'\mathrm{d}\varepsilon_q^p$ around the level of peak stress. Whereupon, after peak state, the assembly is fully mobilized with $1 - \beta$ being equal to 1, indicating that the frictional dissipation energy is accurately represented by $Mp'\mathrm{d}\varepsilon_q^p$. Therefore, the frictional energy of Taylor-Cam Clay type is a good approximation for the range of large shear strain, but needs to be modified as a function of ε_q^p in the range of small shear strain.

From Eq. (40), m can be solved with measured η_d and the corresponding $\varepsilon_{q,d}^p$ at the onset of dilation. Since b' can be regarded as 1, Eq. (40) can be written as

$$\ln\left(\frac{M}{M - \eta_d}\right) = m\varepsilon_{q,d}^p \tag{41}$$

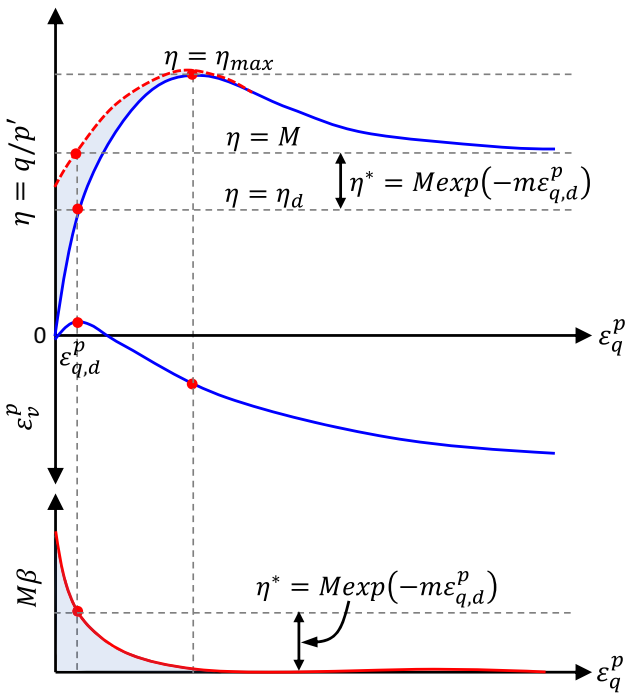

Fig. 13 Schematic illustration of η computed by Eq. (36)

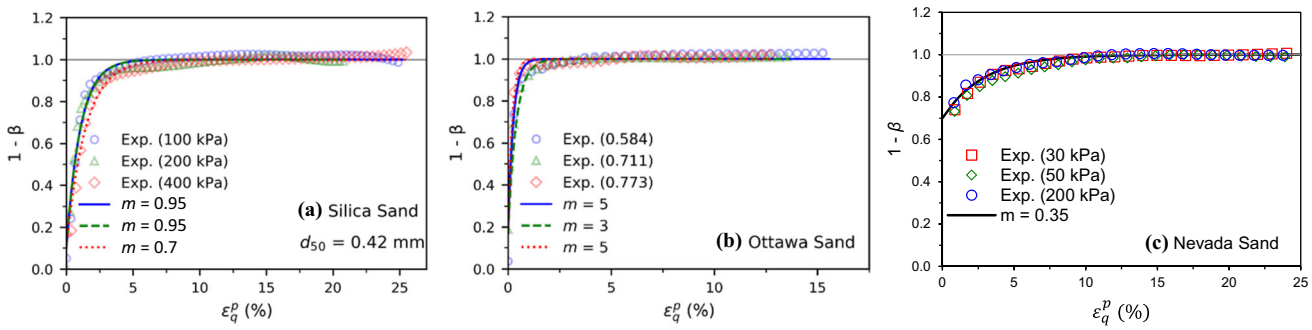

Fig. 14 The curves of beta function for **a** Silica sand, **b** Ottawa sand, and **c** Nevada sand

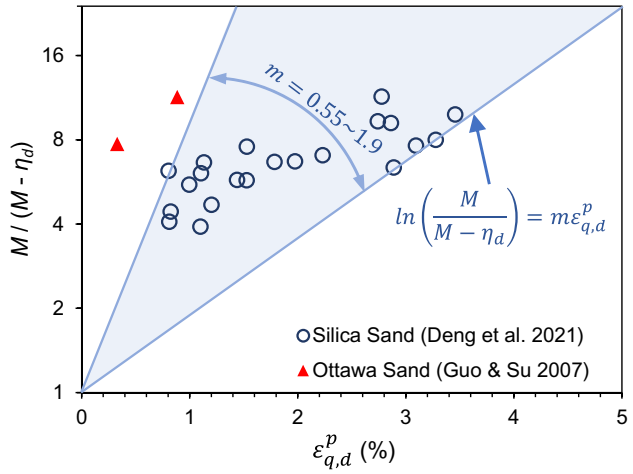

Fig. 15 The relationship of $\ln\left(\frac{M}{M-\eta_d}\right)$ versus shear strain $\varepsilon_{q,d}^p$

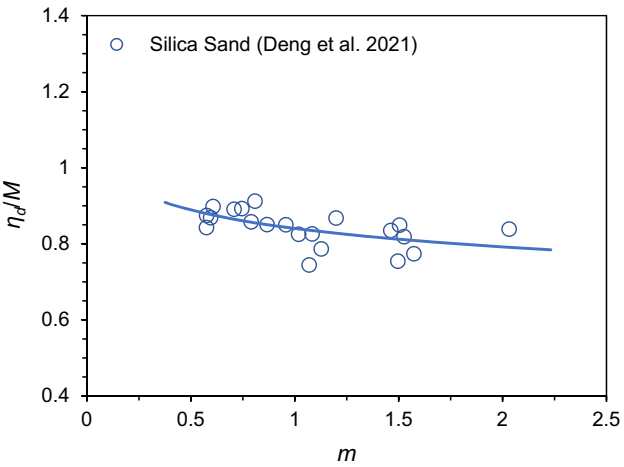

Fig. 16 The correlation between η_d/M and parameter m

Figure 15 shows the measured value of $\ln\left(\frac{M}{M-\eta_d}\right)$ versus $\varepsilon_{q,d}^p$ for Silica sand of seven different particle sizes (see Table 1) and Ottawa sand (see Fig. 3). For a line connecting each data point to the point of origin, its slope is m. The range of m for Silica sand shown in Fig. 15 is about from 0.5 to 2.0.

According to the measured results of the relationship between η_d and $\varepsilon_{q,d}^p$, the calculated value m ranges from 0.5 to 2.0 for silica sand, and from 2.4 to 5 for Ottawa sand. The calculated value of m is also correlated with η_d/M as shown in Fig. 16.

4.5 Summary of the proposed stress–dilatancy relationship

Based on the consideration of a Helmholtz free energy and specific forms of the frictional dissipation energy into the energy equation, a stress–dilatancy relationship was derived and summarized in Table 2.

5 Model evaluation

The comparison of predicted and measured stress–dilatancy relationship is shown in Fig. 17a for dense silica sand (#30–#50) with three confining stresses, Fig. 17b for Ottawa sand with three initial densities, and Fig. 17c for loose Nevada sand with three confining stresses. The predicted stress-dilatancy curve is computed based on the measured volume strain versus shear strain curve. For all dense sands, the dilatancy curves are not linear lines. The curves show similar patterns of back-hook after peak point for various densities and confining stresses, but the curves show different magnitude of $D_{\max}$.

Using the proposed stress–dilatancy relationship (Eq. 36), the predicted stress-dilatancy curves capture the back-hook features and are in good agreement with the measured results. The proposed stress-dilatancy model reduces to Nova's model when $\beta\left(\varepsilon_q^p\right) = 0$, (i.e. Equation 28) and further reduces to Cam Clay model when $N = 0$ (i.e. Equation 29). In Fig. 17, the measured data are also compared with those predicted by Cam Clay, modified Cam Clay models and Nova's model. Note that the stress–

Table 2 Summary for the proposed stress–dilatancy relationship

Description	Equations or parameters
Proposed stress–dilatancy relationship	$D = \frac{1}{1-N}(\eta - (1-\beta)M)$
Dilation	$D = -\mathrm{d}\varepsilon_v^p/\mathrm{d}\varepsilon_q^p$
Stress ratio	$\eta = q/p'$
Correction parameter for frictional dissipation energy	$\beta = \exp\left(-m\varepsilon_q^p\right)$
Required parameters	M: Critical state stress ratio
	N: Helmholtz free energy coefficient
	m: Correction exponent for frictional dissipation energy

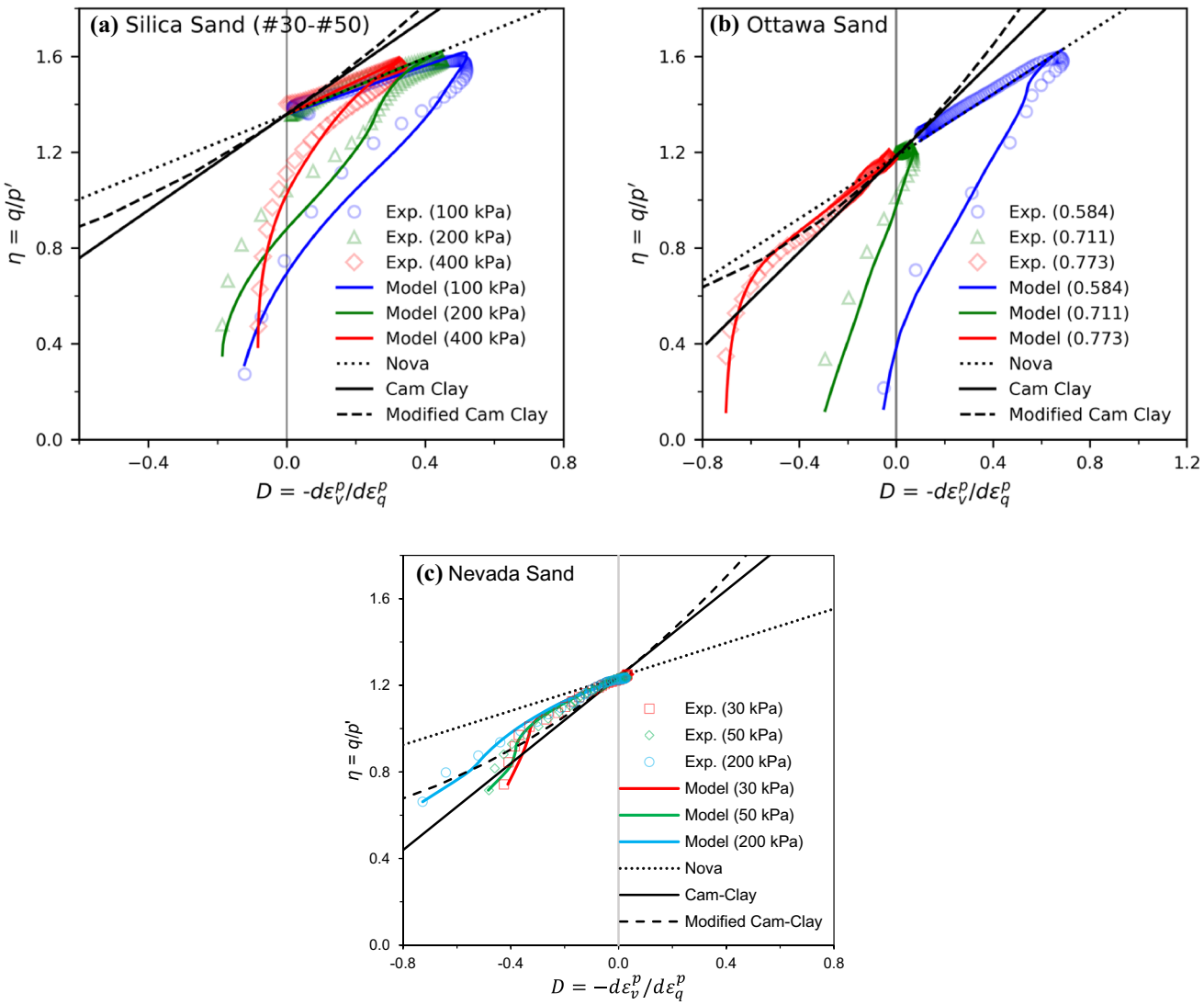

Fig. 17 Predicted Stress-dilatancy curves for **a** Silica sand, **b** Ottawa sand, and **c** Nevada sand, compared with measure results and other models

dilatancy relationship of modified Cam Clay model (Eq. 20) is in the same form as that derived by Collins and Kelly [10]. The stress–dilatancy relationship of Nova's model (Eq. 22) is in the same form as that derived by Jefferies [25]. The modified Cam Clay model gives a curve line, predicting more contraction and less dilation

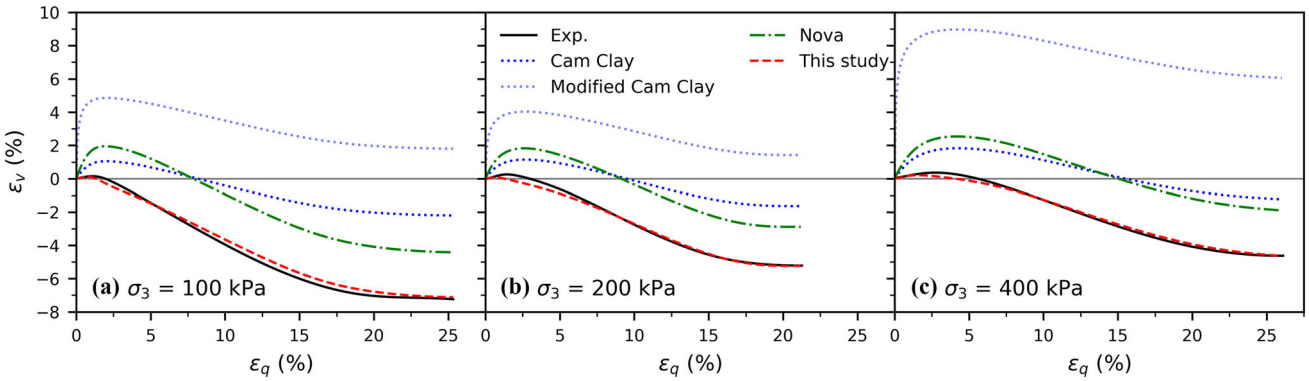

Fig. 18 Predicted volume strain curve for Silica sand compared with measure results and other models

compared with the linear line predicted by Cam Clay model. The Nova's model also gives a linear line with its slope fitting to the post-peak portion. All the three models cannot capture the portion of curves prior to peak state.

To further evaluate the accuracy of the model, we compare the predicted and measured evolution of volume strain. The predicted $\varepsilon_q - \varepsilon_v$ strain curves are computed based on the measured $\varepsilon_q - q$ strain curve. The predicted results are shown for Silica sand (#30–#50 particle size) with three different confining stresses in Fig. 18. The curve predicted by modified Cam Clay model, Cam Clay model, and Nova's model do not agree with the measured curves. Among the three models, Nova's model predicts better curve shape after peak stress state (about $\varepsilon_q = 7\%$). However, due to the discrepancies in the region before the peak point, the Nova's model does not provide good overall predictions. The proposed model predicts curves in good agreement with the measured curves over all range of strain.

The predicted results are shown for Ottawa sand with three different initial densities in Fig. 19. Similar discrepancies are displayed in curves predicted by modified Cam Clay model, Cam Clay model, and Nova's model. Likewise, the Nova's model gives good prediction for the curve

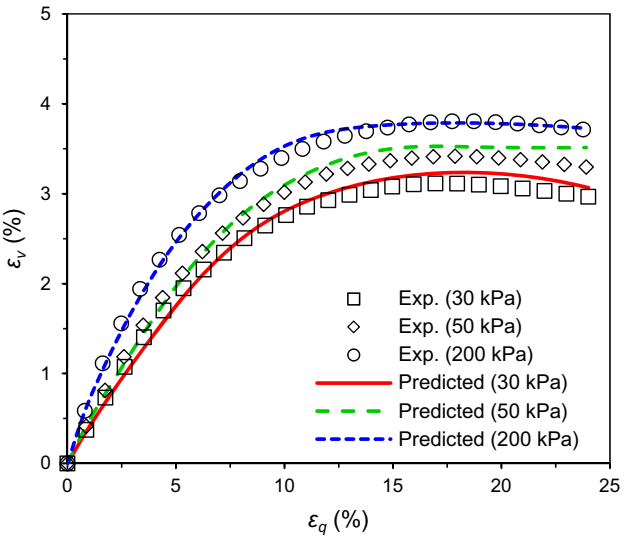

Fig. 20 Predicted volume strain curve for Ottawa sand compared with measure results and other models

shape after peak stress state. The proposed model predicts curves in good agreement with the measured curves. The good performance of the proposed model is also demonstrated by the predictions for loose Nevada sand shown in Fig. 20.

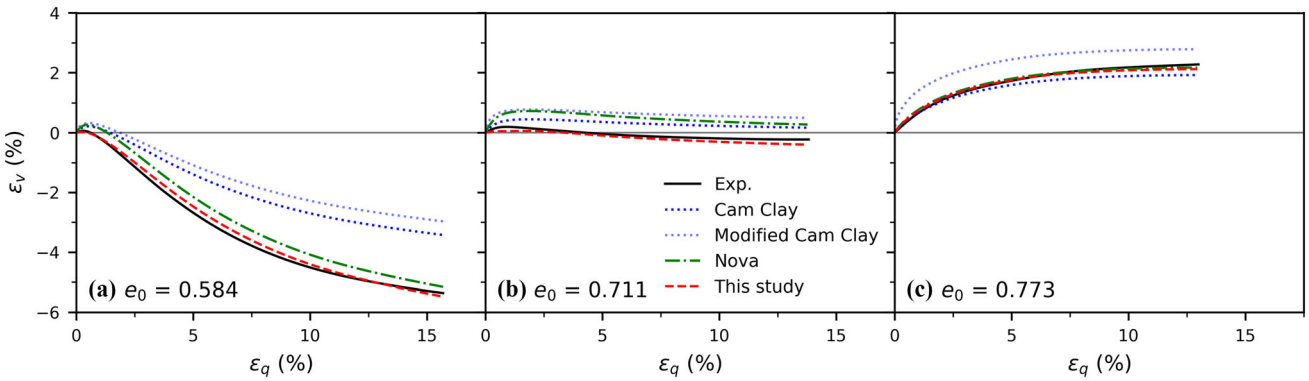

Fig. 19 Predicted volume strain curve for Ottawa sand compared with measure results and other models

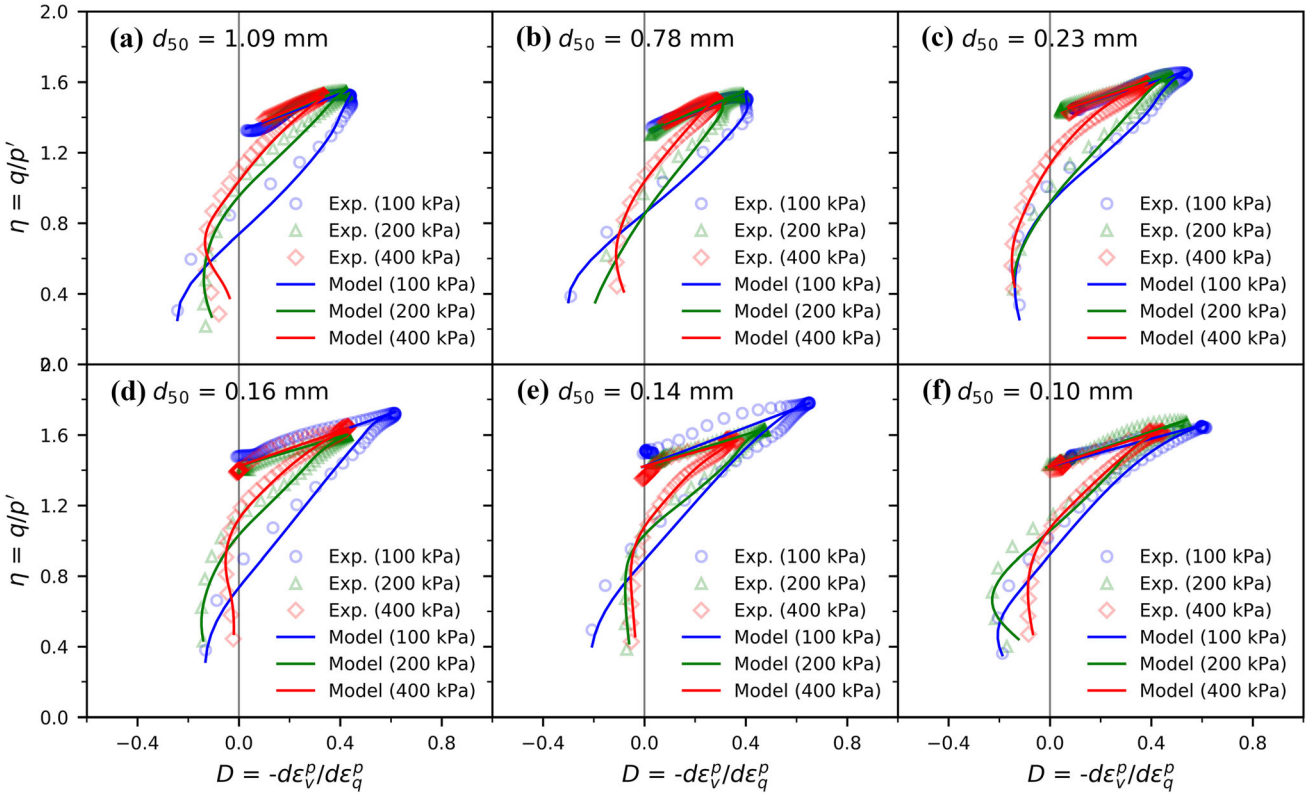

Fig. 21 Predicted stress–dilatancy relationships compared with measure results for Silica sand with different particle sizes

The proposed model is also applied to the other 18 tests on Silica sand with different particle sizes (see Table 1). The predicted results in Fig. 21 show similar back-hook patterns. The predicted pre-peak curves have a good overall agreement with the measured stress-dilatancy curves. Thus, the predicted results of volume strain evolution match well with the measured results. It is noted that for samples with small particle size (0.23 mm–1.09 mm), the occurrence of shear band was observed at the end of test. For these samples, the critical state stress ratios were determined by a multiple-test method for dense sand suggested by several investigators [16, 21, 26, 46, 59]. Appendix B is provided to evaluate the localization effect.

6 Discussion

The classic energy equation of Taylor-Cam Clay type considers only frictional dissipation energy, and involves only one parameter (i.e. critical state stress ratio M). This parameter assures the energy balance at the critical state as shown from the experimental results in Figs. 4, 5 and 6. In the proposed energy equation, for achieving a better energy balance, we have: (1) considered the Helmholtz free energy, and (2) modified the expression of frictional dissipation energy. Accordingly, besides the critical state parameter M, it involves two more parameters (N and m), which are associated with the peak stress state $\eta_{\max}$ and the phase transformation state η_d. The energy balance is assured for the three levels of shear deformation: the phase transformation state, the peak state, and the critical state.

A parametric comparison is given below to show the effect of parameters N and m on a dense sand. Figure 22a shows the predicted stress-dilatancy curves for $m = 0.95$, $N = 0 \sim 0.75$. The predicted stress-dilatancy curves are computed based on the measured volume strain versus shear strain curve for Silica sand (#30–#50 particle size) with 100 kPa confining stress. The value of N does not have effect on the curves prior to the phase transformation state, but considerably alters the slopes after the peak state. The effect of m on the predicted stress-dilatancy curves is shown in Fig. 22b for $N = 0.49$, $m = 0.5 \sim 2$. The value of m does not have effect on the post-peak curve, but significantly alters the curve shape before peak.

Correspondingly, Fig. 23a shows the predicted volume-shear strain curves for $m = 0.95$, $N = 0 - 0.75$. In this case, the predicted volume-shear strain curves are computed based on the measured stress versus shear strain curve for Silica sand (#30–#50 particle size) with 100 kPa confining stress. The value of N does not have effect on the curves prior to the phase transformation state, but significantly influences the slopes of volumetric-shear strain

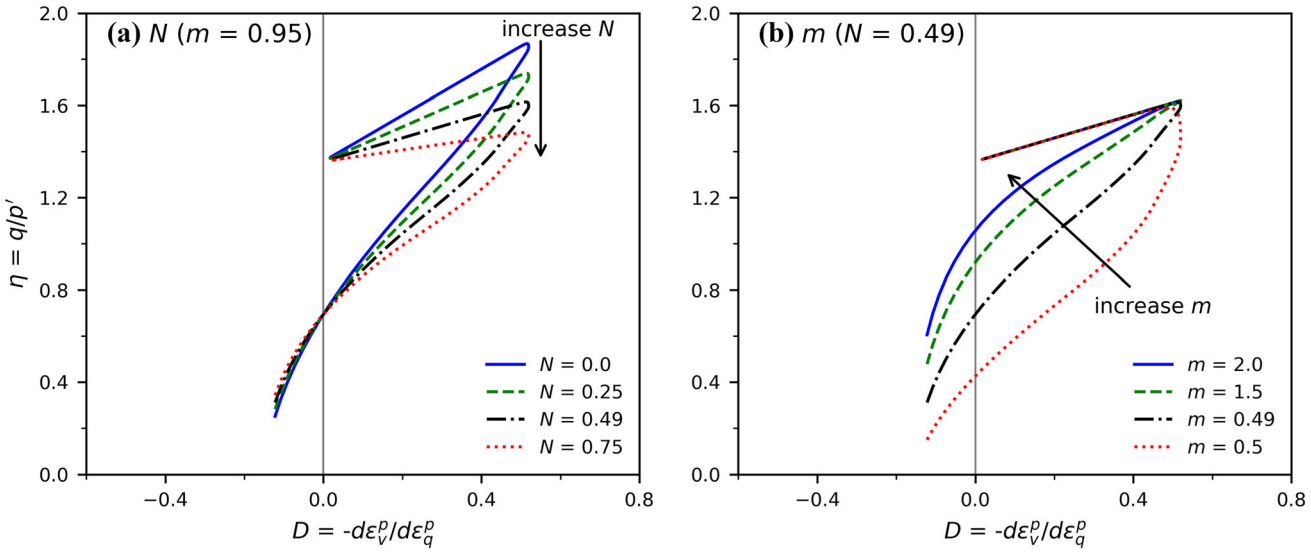

Fig. 22 Parametric comparisons of predicted stress–dilatancy relationships for dense sand: **a** various N keeping $m = 0.95$, and **b** various m keeping $N = 0.49$

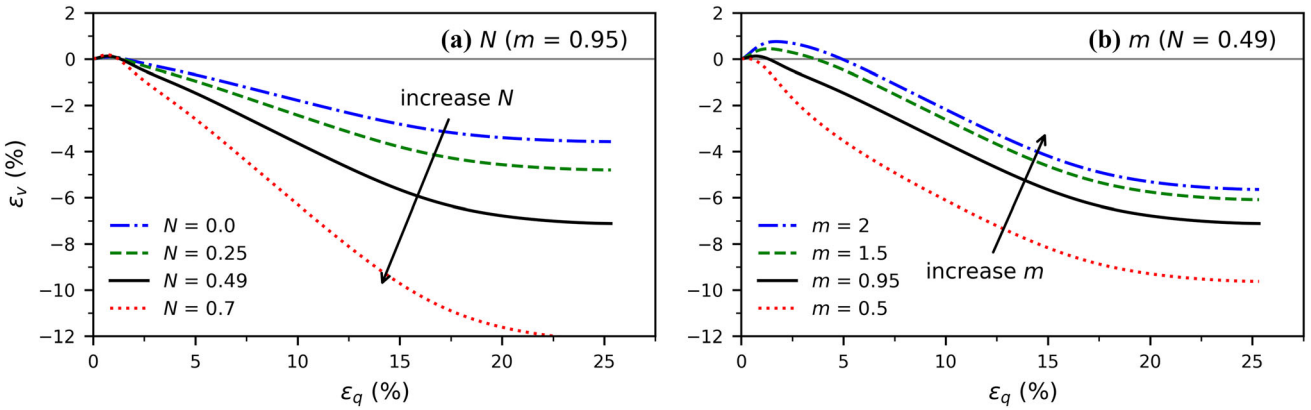

Fig. 23 Parametric comparisons of predicted volume versus shear strain relationships for dense sand: **a** various N keeping $m = 0.95$, and **b** various m keeping $N = 0.49$

curves after the peak state (about 7% of ε_q). The effect of m on the predicted volume-shear strain curves is shown in Fig. 23b for $N = 0.49$, $m = 0.5 \sim 2$. In Fig. 23b, the slopes of volumetric-shear strain curves after the peak state are nearly parallel for various values of m. The value of m, however, substantially influences on the slopes prior to the phase transformation state.

A parametric comparison is also given to show the effect of parameters N and m on loose sand. Figure 24a shows the predicted stress-dilatancy curves for $m = 5.0$, $N = 0 \sim 0.75$. The predicted stress-dilatancy curves are computed based on the measured volume strain versus shear strain curve for Ottawa sand with void ratio 0.773 (very loose condition). The effect of N mainly alters the slopes at higher stress level ($\eta > 0.8$). Effect of m is shown in Fig. 24b for the predicted curves with $N = 0.22$, $m = 1 \sim 10$. The value of m does not have effect on the curve at higher stress level, but considerably alters the curve shape at lower stress level.

Similarly, Fig. 25a shows the predicted volume-shear strain curves for $m = 5$, $N = 0 \sim 0.75$. In this case, the predicted volume-shear strain curves are computed based on the measured stress versus shear strain curve for the very loose Ottawa sand. The value of N significantly influences on the slopes of volumetric-shear strain curves over all strain range. Figure 25b shows the predicted curves for $N = 0.22$, $m = 1 \sim 10$. In Fig. 25b, the slopes of volumetric-shear strain curves, in the range of $\varepsilon_q > 3\%$, are parallel for various values of m. The value of m, however, considerably influences the slopes of curves in the range of $\varepsilon_q < 3\%$.

The quantities of $\eta_{\max}$ and η_d influenced by confining stress and soil density are vital to the stress-dilatancy behavior. The two parameters $(\eta_{\max} - M)$ and $(\eta_d - M)$

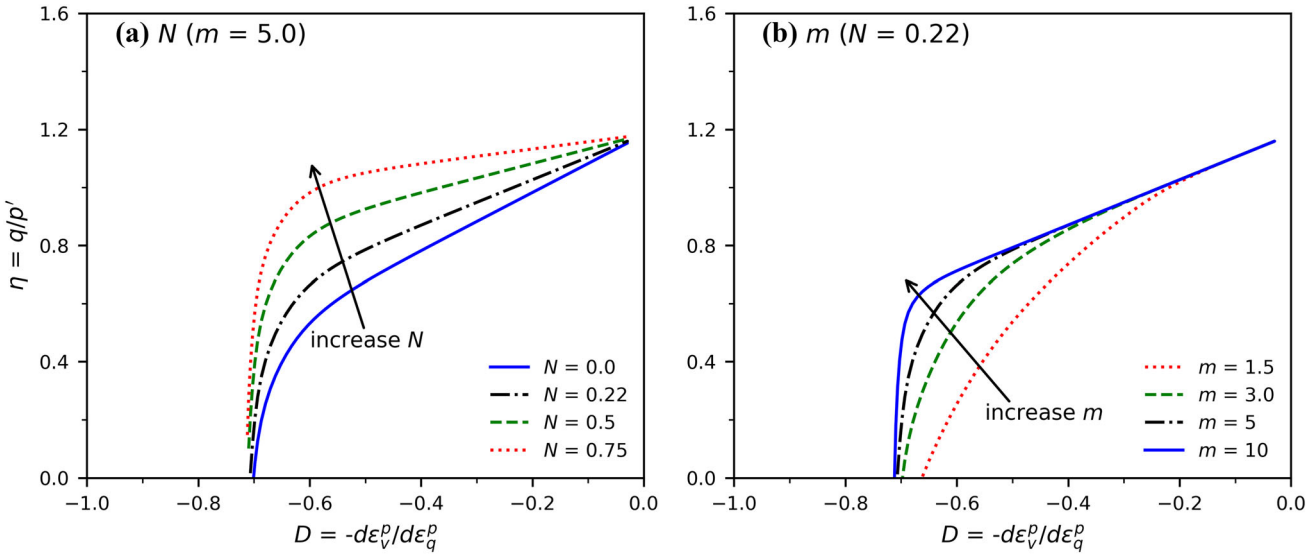

Fig. 24 Parametric comparisons of predicted stress–dilatancy relationships for very loose sand: **a** various N keeping $m = 5$, and **b** various m keeping $N = 0.22$

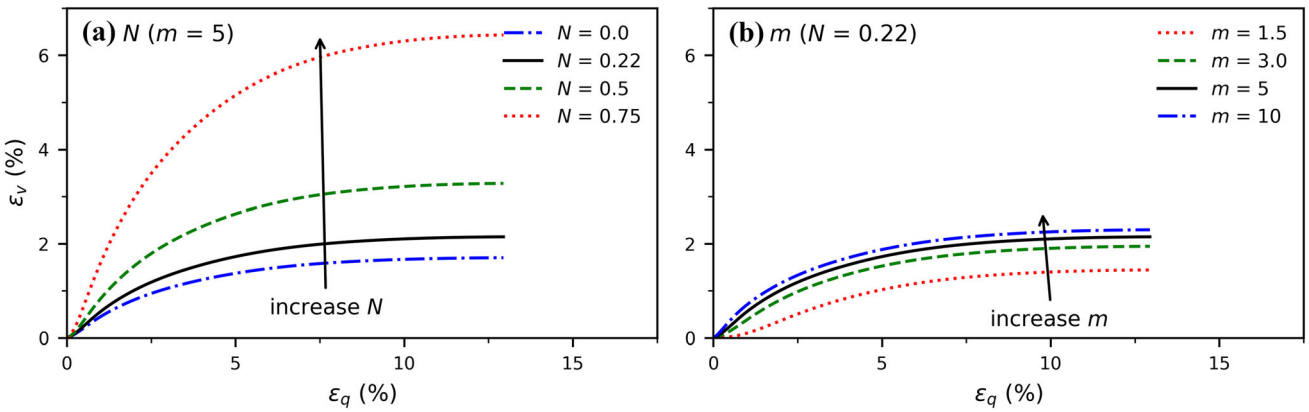

Fig. 25 Parametric comparisons of predicted volume versus shear strain relationships for very loose sand: **a** various N keeping $m = 5$, and **b** various m keeping $N = 0.22$

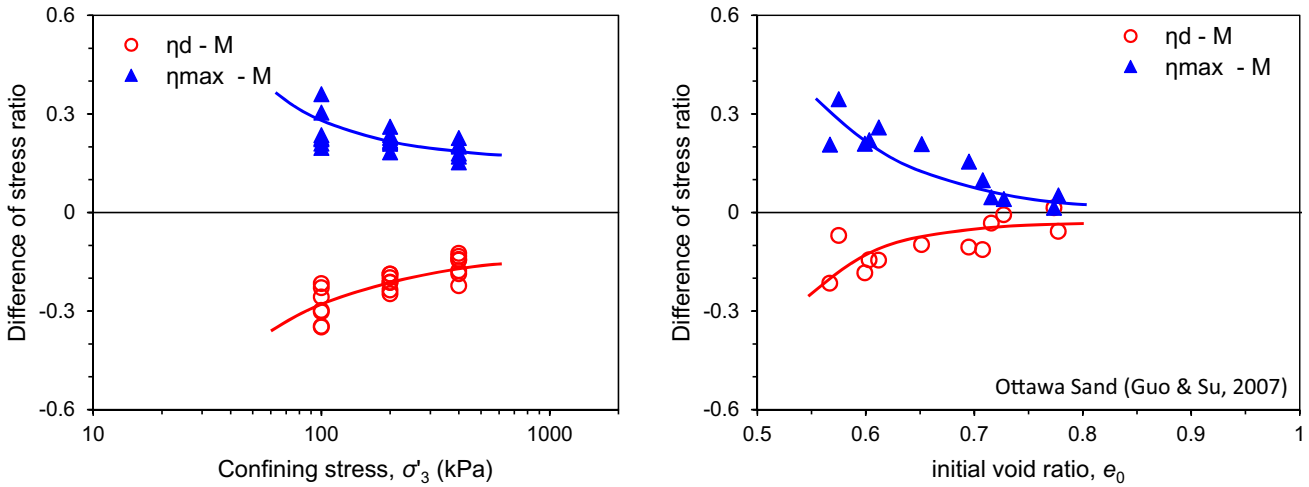

Fig. 26 The on-set stress η_d and peak stress η_{max} influenced by confining stress and density

for Silica sand are plotted in Fig. 26a as a function of confining stress. These two curves have exponential shape approaching to the base line. These two parameters $(\eta_{\max} - M)$ and $(\eta_d - M)$ for Ottawa sand are also plotted in Fig. 26b as a function of density, which have similar patterns as those in Fig. 26a. The effects of density on the peak state friction angle and the phase transformation state friction angle have been studied by many investigators [16, 19, 21, 34] in abundant references. Thus, using the present model, the stress-dilatancy behavior can be conveniently studied for the effect of density and confining stress.

7 Summary and conclusion

In this study, energy equation of Taylor-Cam Clay type is investigated for sand without particle breakage. In addition to the frictional dissipation, we considered the Helmholtz free energy originated from the dilation due to force chain buckling. This essential physics mechanism is missed in the classic stress-dilatancy models. We also found that energy equation of Taylor-Cam Clay type does not satisfy the energy conservation. The frictional dissipation energy is overestimated for the small shear stress level, particularly in dense sand. The discrepancies of energy balance need to be corrected in order to predict correctly the dilatancy behavior. The proposed model is evaluated using experimentally measured results. It shows that the model can correctly capture the back-hook features of stress-dilatancy and can predict the evolution of volume with excellent agreement with measured results.

Two parameters N and m for this model can be calibrated from the measured stress ratios at peak state and at phase transformation state in a triaxial test. The stress ratios, η_d and $\eta_{\max}$, influenced by density and confining pressure have been extensively studied in the literature. Thus, the model provides a tool for further study the dilatancy behavior influenced by density and confining pressure.

Appendix A: Evaluating the coupling effect

The common assumption in elastoplastic theory is adopted to decompose the strain into elastic and plastic parts (denoted by 'e' and 'p' superscripts), i.e.,

$$\mathrm{d}\varepsilon_q = \mathrm{d}\varepsilon_q^e + \mathrm{d}\varepsilon_q^p,\ \mathrm{d}\varepsilon_v = \mathrm{d}\varepsilon_v^e + \mathrm{d}\varepsilon_v^p \tag{A.1}$$

Here, we evaluate the elastic–plastic coupling effect on the calculated results of elastic and plastic strains. Elastic strains follow Hooke's law given as

$$\varepsilon_q^e = \frac{q}{3G}, \varepsilon_v^e = \frac{p'}{K} \tag{A.2}$$

In this study, shear modulus and bulk modulus are considered as a function of void ratio e and applied mean stress p' (see Eqs. 23a and 23b). The function can be expressed as Eqs. (A.3a and A.3b), in which, G_0, K_0, e_0, c_g, p_a and n are constants.

$$G = G(p', e) = G_0 p_a \frac{(c_g - e)^2}{1 + e_0}\left(\frac{p'}{p_a}\right)^n \tag{A.3a}$$

$$K = K(p', e) = \underbrace{\frac{2(1+\nu)}{3(1-2\nu)}}_{K_0} G(p', e) \tag{A.3b}$$

Taking the total derivative on Eq. (A.2) yields

$$\mathrm{d}\varepsilon_q^e = \frac{\mathrm{d}q}{3G} - \frac{q}{3G^2}\left(\frac{\partial G}{\partial p'}\mathrm{d}p' + \frac{\partial G}{\partial e}\mathrm{d}e\right) \tag{A.4a}$$

$$\mathrm{d}\varepsilon_v^e = \frac{\mathrm{d}p'}{K} - \frac{p'}{K^2}\left(\frac{\partial K}{\partial p'}\mathrm{d}p' + \frac{\partial K}{\partial e}\mathrm{d}e\right) \tag{A.4b}$$

where $\frac{\partial G}{\partial p'} = \frac{nG}{p'}$, $\frac{\partial G}{\partial e} = G_0 p_a \left(\frac{p'}{p_a}\right)^n \left(1 - \left(\frac{1+c_g}{1+e}\right)^2\right)$, $\frac{\partial K}{\partial p'} = K_0 \frac{\partial G}{\partial p'}$, $\frac{\partial K}{\partial e} = K_0 \frac{\partial G}{\partial e}$, derived from Eqs. (A.3a and A.3b).

On the right side of Eqs. (A.4a and A.4b), there are two terms for both shear and volumetric elastic strain increments. The second term represents the coupled strain increment. To evaluate the effect of the coupled strain increment, two methods (named "Method 1" and "Method 2") were employed to calculate the elastic and plastic strains in this appendix. In "Method 1", the coupled strain increment is not considered, while in "Method 2", the coupled strain increment is considered. Noted that in the elastoplastic constitutive model, "Method 1" is adopted.

An example is shown for Silica sand (#30–#50, see Table 1) with three different confining stresses. The calculated elastic strains and the calculated plastic strains from both methods are plotted in Fig. 27 and in Fig. 28, respectively. As shown in Fig. 27, there is a considerable difference for the calculated elastic strain from both methods. With the consideration of the coupled strain increment, the calculated elastic strain from "Method 2" is less than that from "Method 1". However, since elastic strain is a small fraction of total strain, the difference of the calculated plastic strain between "Method 1" and "Method 2" is negligible, as shown in Fig. 28.

The plastic energy per unit axial strain at ith strain step in these methods was estimated as follows.

$$\dot{W}_i^p = \frac{q_i\left(\varepsilon_{q,i}^p - \varepsilon_{q,i-1}^p\right) + p_i'\left(\varepsilon_{v,i}^p - \varepsilon_{v,i-1}^p\right)}{\varepsilon_{1,i-1} - \varepsilon_{1,i-1}} \tag{A.5a}$$

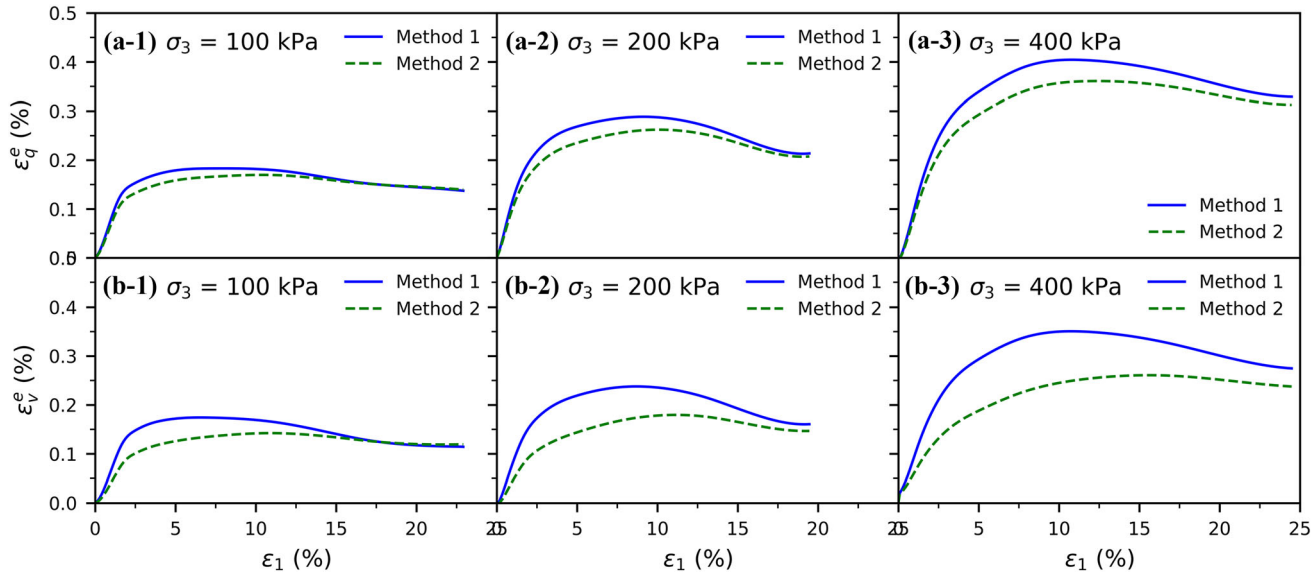

Fig. 27 **a** Elastic shear strain and **b** elastic volumetric strain in "Method 1" and "Method 2"

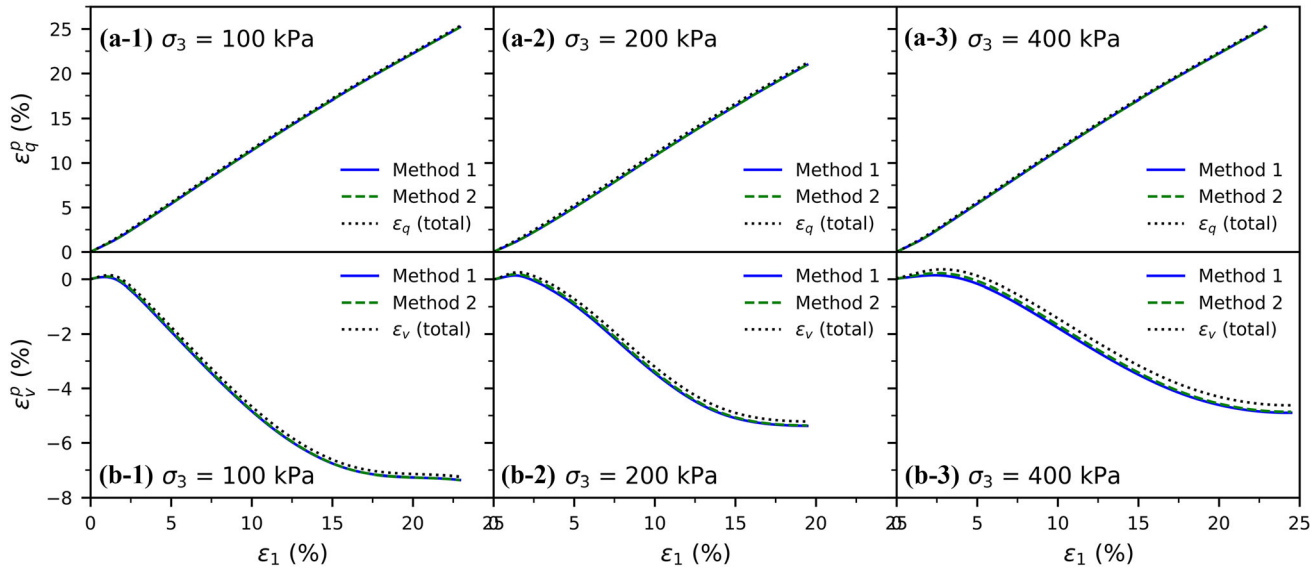

Fig. 28 **a** Plastic shear strain and **b** plastic volumetric strain in "Method 1" and "Method 2"

$$\Phi_i = \frac{\left(1-\beta\left(\varepsilon_{q,i}^p\right)\right) M p_i^{'}\left(\varepsilon_{q,i}^p - \varepsilon_{q,i-1}^p\right)}{\varepsilon_{1,i-1} - \varepsilon_{1,i-1}} \tag{A.5b}$$

$$\dot{\Psi}_i^p = \frac{N p_i^{'}\left(\varepsilon_{v,i}^p - \varepsilon_{v,i-1}^p\right)}{\varepsilon_{1,i-1} - \varepsilon_{1,i-1}} \tag{A.5c}$$

where β is calculated using Eq. (38).

The estimated plastic work, frictional dissipation, and plastic Helmholtz free energies for the Silica sand are plotted in Fig. 29. Due to the trivial difference in the plastic strain between these two methods, the difference in each plastic energy between these two methods is expected to be negligible as shown Fig. 29. Therefore, the effect of coupled strain increment is insignificant with respect to the study of balance of plastic work, frictional dissipation, and plastic Helmholtz free energy.

Appendix B: Evaluating strain localization effect

For some dense sand samples used in this study, strain localization (i.e. shear band or bifurcation) takes place after peak stress. After strain localization occurs, the global stress–strain behavior of the soil is largely dependent on

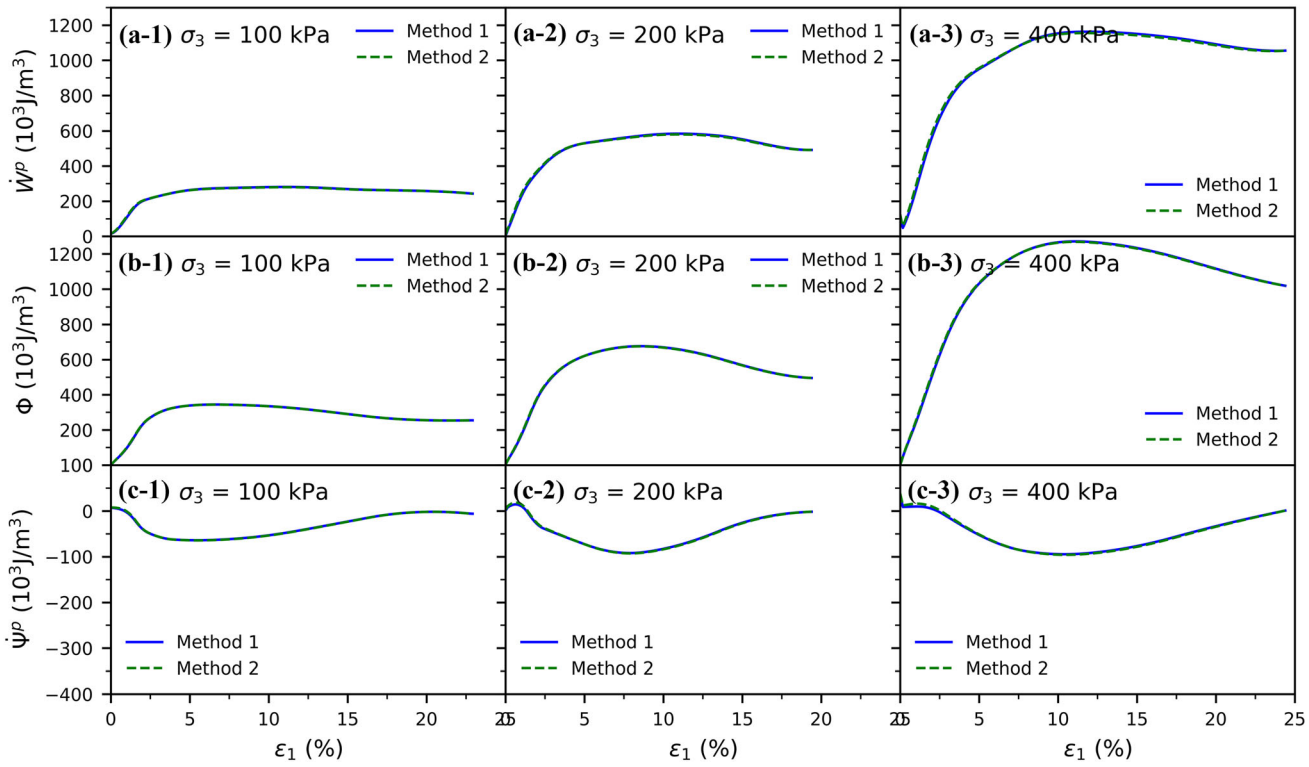

Fig. 29 **a** Plastic work, **b** dissipation energy, and **c** plastic Helmholtz free energy in "Method 1" and "Method 2"

the soil in the shearing zone, which has essentially reached a constant volume state. Therefore, the global stress–strain and volumetric strain curves after the occurrence of shear band would not represent the behavior of uniformly deformed material due to non-homogeneous deformation.

To avoid the influence of localization, Nova [36] and Bolton [4] suggested to determine the stress-dilatancy making use of multiple test samples under different confining pressures or different void ratios for the same granular soil, using the measured peak stress ratios and the corresponding dilatancy. Since, at peak stress state, the localization just starts to develop in a sample, thus the samples can be regarded as uniformly deformed. This method has been adopted by many researchers [16, 21, 26, 46, 59].

In this study, for these samples with shear band, we use test results from three different confining stresses (i.e., 100 kPa, 200 kPa, and 400 kPa) to obtain the relationship between the peak stress ratio and the corresponding dilatancy by fitting the dilation equation (Eq. 31). For the three tests shown in Fig. 30, the fitted solid line from multiple samples is considered to be the stress-dilatancy behavior of

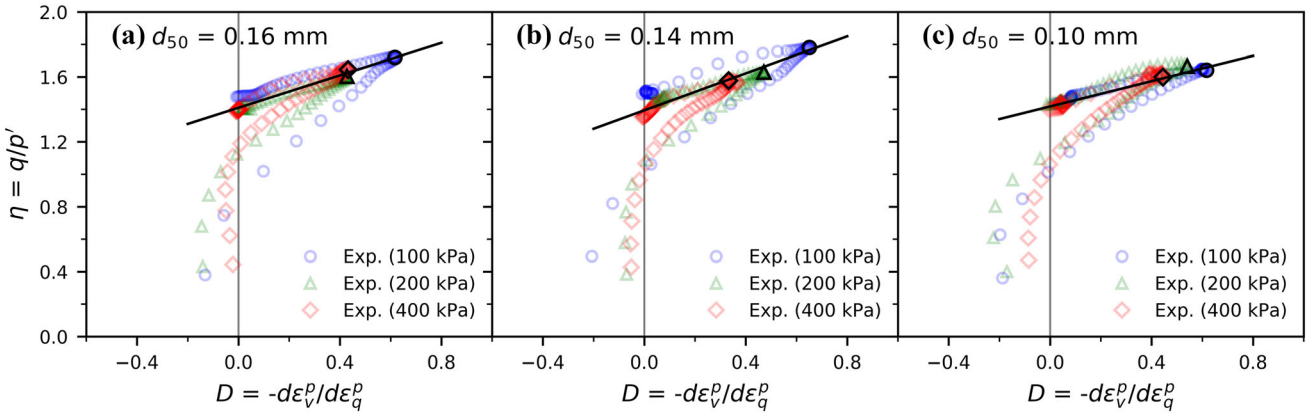

Fig. 30 The post-peak stress-dilatancy responses for the samples with occurrence of strain localization (the symbols are the measured points of three confining pressures for each sand, the black lines are the fitted stress–dilatancy relationship from multiple-test method)

a uniformly deformed sample without localization. Figure 30 shows minor deviations between the post-peak stress-dilatancy responses (data symbols) and the fitted solid line, which means that the critical state stress ratio M needs to be corrected for these tests with localizations.

In the proposed stress-dilatancy model, three parameters are required, M, N, and m (see Sect. 4.5). Among the three parameters, the values of N and m are not influenced by strain localization, because the value of N is obtained from the energy curves considering only peak state. The value of m is obtained mainly from the energy curves before peak state. However, the value M is affected by strain localization, which should be obtained from multiple-test method.

Comparing the predictions shown in Figs. 17 and 30, the predicted curves using the proposed model agree well with the fitted dilatancy relationship from multiple-test method.

Acknowledgements This work was supported by the National Science Foundation of the United States under a research grant (CMMI-1917238). The support is greatly acknowledged.

References

1. Agnolin I, Jenkins JT, La RL (2006) A continuum theory for a random array of identical, elastic, frictional disks. Mech Mater 38:687–701. https://doi.org/10.1016/j.mechmat.2005.06.011
2. Alonso-Marroquín F, Vardoulakis I (2005) Micromechanics of shear bands in granular media. In: Garcia-Rojo R, Herrmann HJ, McNamara S (eds) Powders and grains. Balkerma, Rotterdam, pp 701–704
3. Been K, Jefferies M (2004) Stress-dilatancy in very loose sand. Can Geotech J 41:972–989. https://doi.org/10.1139/t04-038
4. Bolton MD (1986) The strength and dilatancy of sands. Géotechnique 36:65–78. https://doi.org/10.1680/geot.1986.36.1.65
5. Burland JB, Roscoe KH (1969) Local strains and pore pressures in a normally consolidated clay layer during one-dimensional consolidation. Geotechnique 19:335–356. https://doi.org/10.1680/geot.1969.19.3.335
6. Chang CS, Hicher PY (2005) An elasto-plastic model for granular materials with microstructural consideration. Int J Solids Struct 42:4258–4277. https://doi.org/10.1016/j.ijsolstr.2004.09.021
7. Collins IF (2005) The concept of stored plastic work or frozen elastic energy in soil mechanics. Géotechnique 55:373–382. https://doi.org/10.1680/geot.55.5.373.66023
8. Collins IF, Hilder T (2002) A theoretical framework for constructing elastic/plastic constitutive models of triaxial tests. Int J Numer Anal Methods Geomech 26:1313–1347. https://doi.org/10.1002/nag.247
9. Collins IF, Houlsby GT (1997) Application of thermomechanical principles to the modelling of geotechnical materials. Proc R Soc A Math Phys Eng Sci 453:1975–2001. https://doi.org/10.1098/rspa.1997.0107
10. Collins IF, Kelly PA (2002) A thermomechanical analysis of a family of soil models. Géotechnique 52:507–518. https://doi.org/10.1680/geot.52.7.507.38756
11. Collins IF, Muhunthan B (2003) On the relationship between stress-dilatancy, anisotropy, and plastic dissipation for granular materials. Geotechnique 53:611–618. https://doi.org/10.1680/geot.2003.53.7.611
12. Dafalias YF, Manzari MT (2004) Simple plasticity sand model accounting for fabric change effects. J Eng Mech 130:622–634. https://doi.org/10.1061/(asce)0733-9399(2004)130:6(622)
13. Deng Y, Yilmaz Y, Gokce A, Chang CS (2021) Influence of particle size on the drained shear behavior of a dense fluvial sand. Acta Geotech 16:2071–2088. https://doi.org/10.1007/s11440-021-01143-7
14. Dewers TA, Issen KA, Holcomb DJ et al (2017) Strain localization and elastic-plastic coupling during deformation of porous sandstone. Int J Rock Mech Min Sci 98:167–180. https://doi.org/10.1016/j.ijrmms.2017.06.005
15. Guo P (2009) Energy approach towards stress-dilatancy formulation based on double slip-rotation rate concept. Soils Found 49:443–457. https://doi.org/10.3208/sandf.49.443
16. Guo P, Su X (2007) Shear strength, interparticle locking, and dilatancy of granular materials. Can Geotech J 44:579–591. https://doi.org/10.1139/T07-010
17. Gutierrez M, Wang J (2009) Non-coaxial version of Rowe's stress-dilatancy relation. Granul Matter 11:129–137. https://doi.org/10.1007/s10035-008-0124-0
18. Hanley KJ, Huang X, O'Sullivan C (2018) Energy dissipation in soil samples during drained triaxial shearing. Géotechnique 68:421–433. https://doi.org/10.1680/jgeot.16.P.317
19. Hanna A (2001) Determination of plane-strain shear strength of sand from the results of triaxial tests. Can Geotech J 38:1231–1240. https://doi.org/10.1139/cgj-38-6-1231
20. Hardin BO, Drnevich VP (1972) Shear modulus and damping in soils: design equations and curves. J Soil Mech Found Div 98:667–692. https://doi.org/10.1061/jsfeaq.0001760
21. Harehdasht SA, Karray M, Hussien MN, Chekired M (2017) Influence of particle size and gradation on the stress-dilatancy behavior of granular materials during drained triaxial compression. Int J Geomech 17:04017077. https://doi.org/10.1061/(ASCE)GM.1943-5622.0000951
22. Houlsby GT, Puzrin AM (2000) Thermomechanical framework for constitutive models for rate-independent dissipative materials. Int J Plast 16:1017–1047. https://doi.org/10.1016/S0749-6419(99)00073-X
23. Iwashita K, Oda M (2000) Micro-deformation mechanism of shear banding process based on modified distinct element method. Powder Technol 109:192–205
24. Jefferies MG (1993) Nor-Sand: a simle critical state model for sand. Geotechnique 43:91–103. https://doi.org/10.1680/geot.1993.43.1.91
25. Jefferies M (1997) Plastic work and isotropic softening in unloading. Geotechnique 47:1037–1042
26. Jewell RA (1989) Direct shear tests on sand. Geotechnique 39:309–322
27. Jong DJD, G, (1976) Rowe's stress–dilatancy relation based on friction. Geotechnique 26:527–534. https://doi.org/10.1680/geot.1976.26.3.527
28. Kruyt NP, Rothenburg L (2006) Shear strength, dilatancy, energy and dissipation in quasi-static deformation of granular materials. J Stat Mech Theory Exp. https://doi.org/10.1088/1742-5468/2006/07/P07021
29. Lemaitre J, Chaboche JL (1990) Mechanics of solid materials. Cambridge University Press, Cambridge
30. Li XS, Dafalias YF (2000) Dilatancy for cohesionless soils. Geotechnique 50:449–460. https://doi.org/10.1680/geot.2000.50.4.449
31. Lin W, Liu A, Mao W, Koseki J (2020) Acoustic emission characteristics of a dry sandy soil subjected to drained triaxial compression. Acta Geotech 15:2493–2506. https://doi.org/10.1007/s11440-020-00932-w

32. Misra A, Chang CS (1993) Effective elastic moduli of heterogeneous granular solids. Int J Solids Struct 30:2547–2566. https://doi.org/10.1016/0020-7683(93)90165-4
33. Newland PL, Allely BH (1957) Volume changes in drained triaxial tests on granular materials. Geotechnique 7:17–34. https://doi.org/10.1680/geot.1957.7.1.17
34. Norris GM (1977) The drained shear strength of uniform quartz sand as related to particle size and natural variation in particle shape and surface roughness. Ph.D. thesis, University of California, Berkeley
35. Norris G, Siddharthan R, Zafir Z, Madhu R (1997) Liquefaction and residual strength of sands from drained triaxial tests. J Geotech Geoenviron Eng 123:220–228. https://doi.org/10.1061/(asce)1090-0241(1997)123:3(220)
36. Nova R (1982) A constitutive model under monotonic and cyclic loading. In: Pande G, Zienkiewicz OC (eds) Soil mechanics—transient and cyclic loads. John Wiley & Sons Ltd, New York, pp 343–373
37. Oda M, Kazama H (1998) Microstructure of shear bands and its relation to the mechanisms of dilatancy and failure of dense granular. Geotechnique 48:465–481
38. Oda M, Konishi J, Nemat-Nasser S (1982) Experimental micromechanical evaluation of strength of granular materials: effects of particle rolling. Mech Mater 1:269–283. https://doi.org/10.1016/0167-6636(82)90027-8
39. Powrie W, Ni Q, Harkness RM, Zhang X (2005) Numerical modelling of plane strain tests on sands using a particulate approach. Géotechnique 55:297–306. https://doi.org/10.1680/geot.2005.55.4.297
40. Roscoe KH, Burland JB (1968) On the generalised stress-strain behaviour of 'wet' clay. In: Heyman J, Leckie F (eds) Engineering plasticity. Cambridge University Press, Cambridge, pp 535–609
41. Roscoe KH, Schofield AN, Thurairajah A (1963) Yielding of clays in states wetter than critical. Geotechnique 13:211–240. https://doi.org/10.1680/geot.1963.13.3.211
42. Roux JN (2000) Geometric origin of mechanical properties of granular materials. Phys Rev E—Stat Phys Plasmas Fluids Relat Interdiscip Top 61:6802–6836. https://doi.org/10.1103/PhysRevE.61.6802
43. Rowe PW (1962) The stress dilatancy relation for static equilibrium of an assembly of particles in contact. Proc R Soc 269A:500–527
44. Schanz T, Vermeer PA (1996) Angles of friction and dilatancy of sand. Géotechnique 46:145–151. https://doi.org/10.1680/geot.1996.46.1.145
45. Schofield AN, Wroth CP (1968) Critical state soil mechanics. McGraw-Hill, Maidenhead
46. Simoni A, Houlsby GT (2006) The direct shear strength and dilatancy of sand-gravel mixtures. Geotech Geol Eng 24:523–549. https://doi.org/10.1007/s10706-004-5832-6
47. Smith A, Dixon N (2019) Acoustic emission behaviour of dense sands. Geotechnique 69:1107–1122. https://doi.org/10.1680/jgeot.18.P.209
48. Szypcio Z (2016) Stress-dilatancy for soils. Part I: the frictional state theory. Stud Geotech Mech 38:51–57. https://doi.org/10.1515/sgem-2016-0030
49. Talyor DW (1948) Fundamentals of soil mechanics. John Wiley & Sons Inc, New York
50. Tordesillas A, Shi J, Tshaikiwsky T (2006) Stress-dilatancy and force chain evolution. Int J Numer Anal Methods Geomech 30:1303–1336. https://doi.org/10.1002/nag
51. Tordesillas A, Walsh SDC (2005) Analysis of deformation and localization in thermomicromechanical Cosserat models of granular media. Powders Grains. https://doi.org/10.1201/noe0415383486
52. Ulm F-J, Coussy O (2003) Mechanics and durability of solids, 1st edn. Prentice Hall, Hoboken
53. Vardoulakis I, Georgopoulos I (2005) The "stress-dilatancy" hypothesis revisited: shear-banding related instabilities. Soils Found 45:61–76
54. Vermeer PA, de Borst R (1984) Non-associated plasticity for soils, concrete and rock. HERON 29:1–64
55. Walsh SDC, Tordesillas A, Peters JF (2007) Development of micromechanical models for granular media: the projection problem. Granul Matter 9:337–352. https://doi.org/10.1007/s10035-007-0043-5
56. Wan RG, Guo PJ (1998) A simple constitutive model for granular soils: modified stress-dilatancy approach. Comput Geotech 22:109–133
57. Wan RG, Guo PJ (1999) A pressure and density dependent dilatancy model for granular materials. Soils Found 39:1–11
58. Wood DM (1991) Soil behaviour and critical state soil mechanics. Soil Behav Crit State Soil Mech. https://doi.org/10.1017/CBO9781139878272
59. Yilmaz Y, Deng Y, Chang CS, Gokce A (2021) Strength-dilatancy and critical state behaviours of binary mixtures of graded sands influenced by particle size ratio and fines content. Geotechnique. https://doi.org/10.1680/jgeot.20.p.320(Accepted)
60. Zhang L, Nguyen NGH, Lambert S et al (2017) The role of force chains in granular materials: from statics to dynamics. Eur J Environ Civ Eng 21:874–895. https://doi.org/10.1080/19648189.2016.1194332